In re: Oil Spill by the Oil Rig "Deepwater Horizon" in the Gulf of Mexico, on April 20, 2010

UNITED STATES DISTRICT COURT
EASTERN DISTRICT OF LOUISIANA
MDL NO. 2179, SECTION J
JUDGE BARBIER; MAGISTRATE JUDGE SHUSHAN

Expert Report of Srdjan Nesic, Ph.D

May 1, 2013

TABLE OF CONTENTS

1. EXECUTIVE SUMMARY

I have been retained on behalf of BP America Inc. to provide expert opinions in connection with litigation arising out of the *Deepwater Horizon* incident of April 20, 2010. Specifically, I have been asked to analyze the effect, if any, of metal erosion on the rate at which hydrocarbons flowed up the production casing of the Macondo well following the incident. Metal erosion is a mechanical process of gradual metal loss caused by repeated impact of solid particles.

As discussed below, metal erosion had a significant effect on flow rate at the Macondo well. Specifically, metal components in the hydrocarbon flow path, including components of the blowout preventer ("BOP") and the kinked riser, obstructed flow in the aftermath of the incident, while sand or other solid particles in the hydrocarbons passing through these metal components gradually eroded these obstructions. The result was a wider flow path enabling a higher flow rate.

Based on my review of materials from this litigation (including physical inspection of eroded Macondo components), computational fluid dynamics ("CFD") modeling, and my education and experience in erosion and the broader field of engineering, I have reached the following opinions with a reasonable degree of scientific certainty:

1. Metal loss due to erosion significantly altered flow restrictions in the BOP and kinked riser through which hydrocarbons passed.
2. Blind Shear Rams ("BSR") and Casing Shear Rams ("CSR") significantly restricted flow before they eroded.
3. When the BSR was activated April 22, 2010, it significantly restricted flow. By the end of the sanding/metal erosion period (assumed to be May 27, 2010, at the time of

Top Kill)[1], the BSR was significantly eroded and no longer substantially restricted flow.

4. When the CSR was activated April 29, it also restricted flow. By the end of the metal erosion period, the CSR was the most significant BOP restriction to flow.

5. The Upper Annular Preventer ("UAP") and kinked riser restricted flow throughout the incident, but never at the levels of the BSR or CSR.

6. Assuming the BOP and the kinked riser were the main restrictions to flow in this period (April 22 - May 27), flow rate at the Macondo well would have almost doubled (increased by 88 ± 2%) from April 22 - May 27 due to erosion. This increase was steady throughout the five-week period.

2. BACKGROUND AND CREDENTIALS

I am a Russ Professor of chemical engineering at Ohio University and the Director of the Institute for Corrosion and Multiphase Flow Technology, one of the largest erosion/corrosion laboratories in the world. I have particular expertise in metallic erosion and corrosion, and I have published more than 70 peer-reviewed papers in leading international journals and monographs on this topic. My curriculum vitae, which includes a list of my publications over the last ten years, is attached as Appendix A.

I was previously qualified as an expert witness in August 2010 in *State of Alaska v. BP Exploration (Alaska)*. I was deposed in that case, but did not testify at trial. I have not testified in any other matter in the past four years.

[1] There is evidence that sanding continued beyond this date. In particular, I am aware of contemporaneous documents reporting that sand was in the hydrocarbon flow well into June 2010. See ADX003-0007575, June 5, 2010 Email from M. Burns to S. Black (warning that sand is in oil and may cause erosion); SDX005-0013242, June 23, 2010 Email from R. Merewether to T. Hunter et al. (estimating 30 bbls of sand production).

I am being compensated $400/hour for preparation of my report and any testimony in this matter, which is my standard hourly rate. Colleagues who provided assistance to me on this matter billed at standard hourly rates ranging from $100/hour to $250/hour. The compensation is not contingent upon the outcome of this litigation.

In forming my opinions, I considered the following materials:

1. Flow geometries before and after erosional damage using:
    1. Computer aided design ("CAD") files of nominal BOP geometries produced by Cameron;
    2. Cloud point files of eroded BSR geometries from original laser scans;
    3. Laser scans of other eroded BOP components;
    4. Laser scans of the eroded kinked riser;
    5. Images of eroded components;
    6. ROV footage depicting flow through the kinked riser; and
    7. Analysis by Nigel Richardson, modeling standoff between BSR blades;[2] and
    8. Physical inspection of the eroded BOP components and riser at the Port Michoud, Louisiana facility (on May 21 and September 27, 2012).
2. Operational parameters such as pressure, temperature, fluid composition, physical properties, and approximate flow rates from:
    1. Intertek reports;
    2. Pencor reports;
    3. The Schlumberger report; and
    4. Flow Rate Technical Group estimates of flow rate.

[2] Nigel Richardson's analysis is attached as Appendix F.

3. Data on solids content in the flowing hydrocarbons from:
    1. Q4000 data;
    2. Internal BP reports prepared by Julian Austin modeling erosion of the kink;
    3. Analysis by Hans Vaziri, BP Distinguished Advisor for Sand Management, estimating upper and lower bounding of sand production at the Macondo well, average sand particle size, and timing and duration of sand production;[3] and
    4. Top kill and junk shot data.

A complete list of materials I considered is included as Appendix B.

In addition, I have reviewed the expert reports submitted by Ronald Dykhuizen, Stewart Griffiths, and Mehran Pooladi-Darvish. I focused on the discussion of erosion in those reports, and my response to their opinions on erosion is set forth in Section 8.

3. SCOPE OF WORK

I analyzed flow through and erosion of metal elements along the hydrocarbon flow path in the Macondo well. The analysis considers likely effects of flow rate on metal erosion and reverse effects of eroded geometries on flow rate.

The key elements I analyzed include:

1. **Elements of the BOP stack** (see Figure 1 below showing a cutaway view of the Deepwater Horizon BOP stack components).

[3] Dr. Vaziri's analysis is attached as Appendix E.

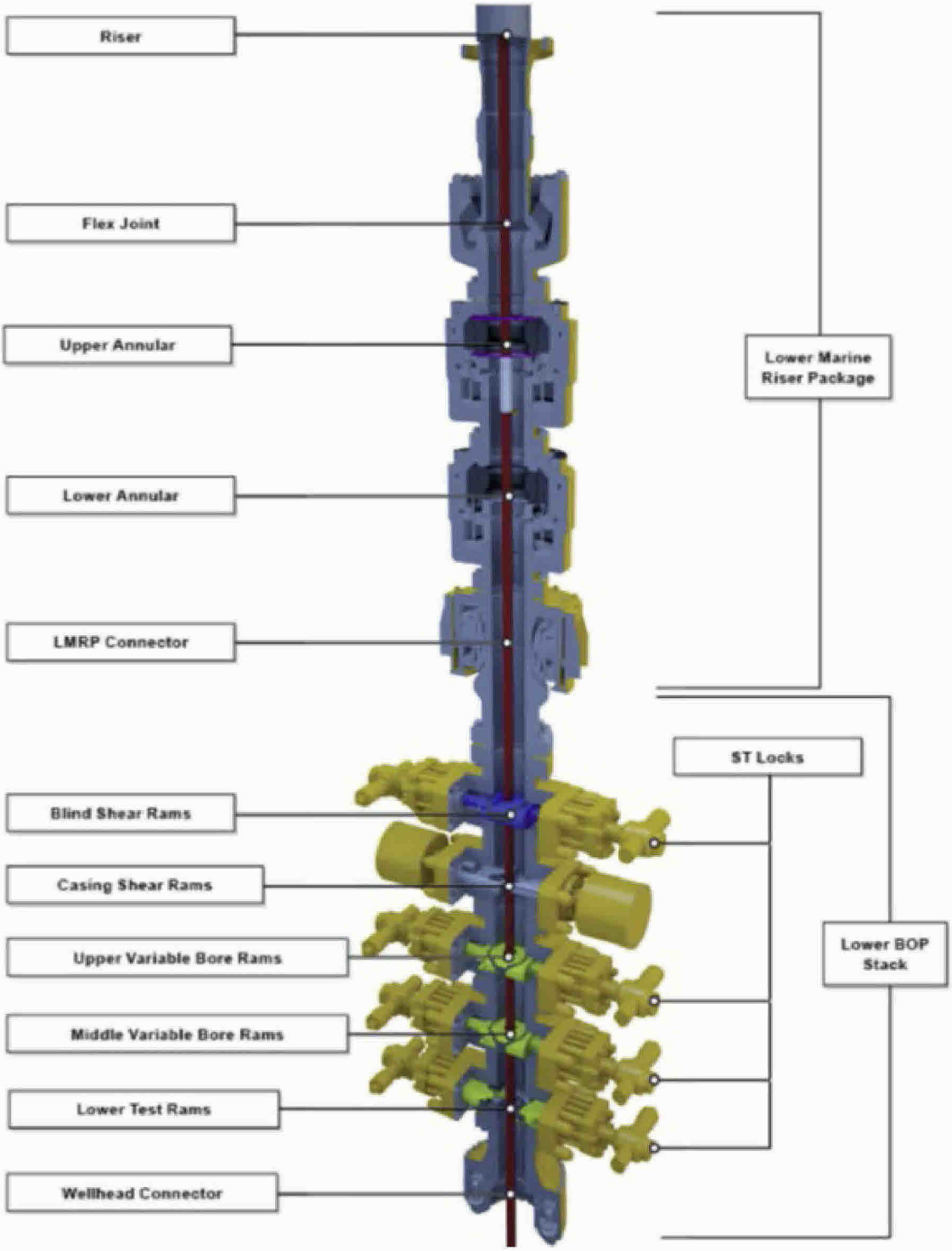

Figure 1. Cutaway view of Deepwater Horizon BOP stack components.

a) **Blind Shear Rams ("BSR")**. BSRs are designed to shear the drill pipe and seal the wellbore. When the BSR at Macondo was activated April 22, it only partially sheared the drill pipe and failed to seal the wellbore completely. The BSR's partial closure significantly restricted hydrocarbon flow, thereby increasing local velocity and turbulence, causing substantial erosion of the BSR blocks, as shown in Figure 2 below.

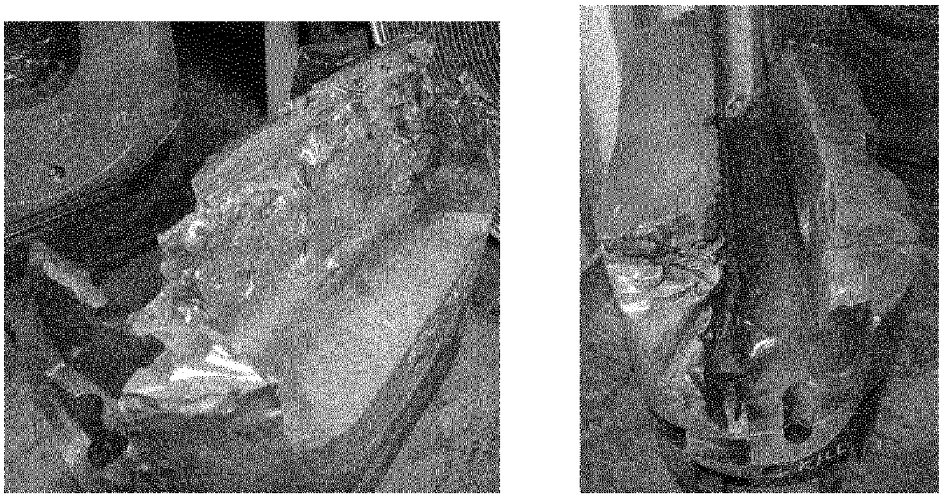

Figure 2. Examples of erosion of the BSR blocks.

b) **Casing Shear Rams ("CSR").** CSRs are designed to shear the casing, but are not intended to seal the wellbore. Nevertheless, when the CSR at Macondo was activated April 29, it significantly restricted hydrocarbon flow, and the recovered CSR blocks reveal significant erosion, as shown in Figure 3 below.

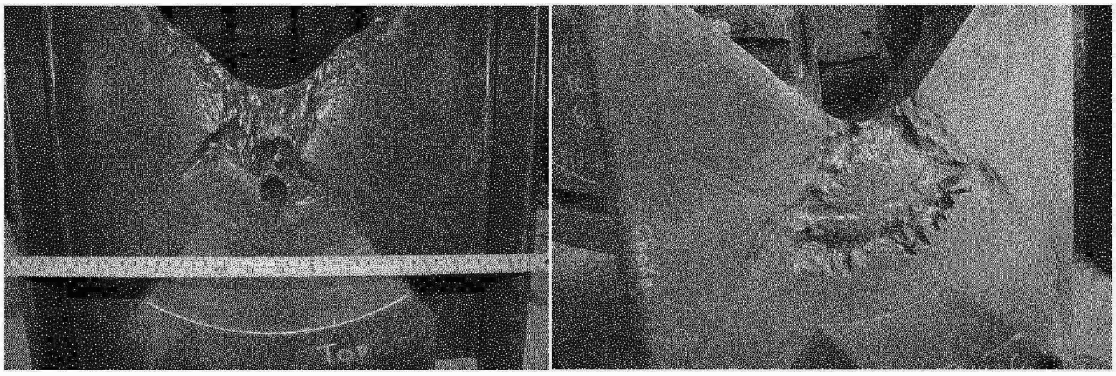

Figure 3. Examples of erosion of the CSR blocks.

c) **Upper Annular Preventer ("UAP").** UAPs are designed to seal the annular space. The UAP at Macondo was activated April 20, but it closed on a tool joint shoulder and only partially sealed the annulus. The UAP's partial seal led to erosion of the elastomer on its fingers and the corresponding section of drill pipe.

4. **Kinked riser**. Risers connect offshore platforms to subsea wellheads. When the *Deepwater Horizon* rig sank April 22, it caused the base of the riser to form an approximately 90-degree kink. Erosion led to formation of holes and leaks in the kinked riser, as seen in Figure 4 below.

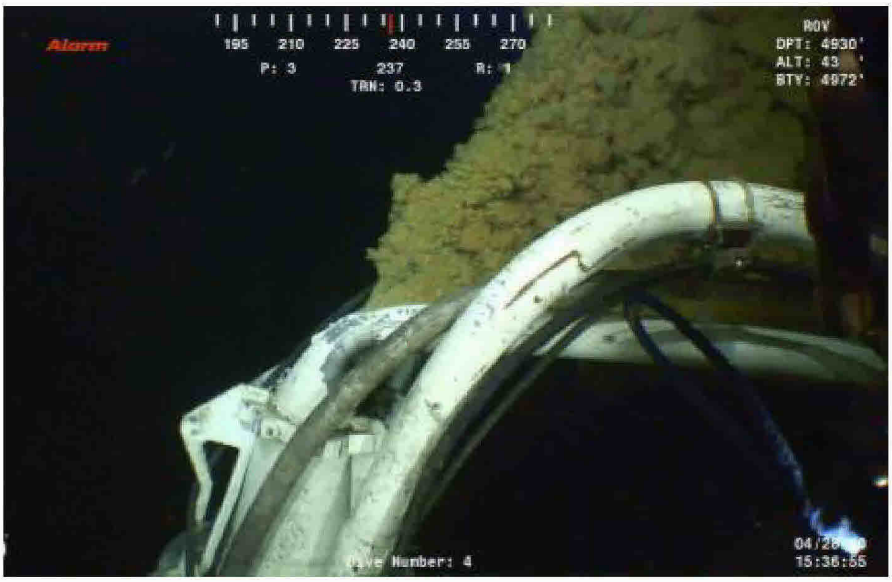

Figure 4. Photograph of leaks in kinked riser, taken April 28, 2010.

4. METHODOLOGY AND EXECUTION

I applied Computational Fluid Dynamics ("CFD")[4] to determine effects of erosion on hydrocarbon flow rate. My analysis is based on numerical simulations of flow of a multiphase mixture (oil, gas, and solid particles) through geometries of interest, accompanied by simulation of the associated erosion process.

For these simulations, I selected ANSYS Fluent flow modeling software. Fluent is one of the leaders in the CFD field, with capabilities spanning applications across a range of industries. I selected this software because of its reputation for stability, accuracy, and flexibility in addressing complex flow geometries such as those modeled here and its potential to work with custom add-on models.

As part of my analysis, I completed the following steps for each simulated component:

- Defined the operational and physical parameters to be used in the simulations;
- Identified and adjusted the simulated flow geometry using a CAD package;
- Imported the flow geometry into Fluent, created a mesh, and defined boundary conditions;
- Simulated flow and erosion scenarios;
- Produced numerical and graphical outputs; and
- Analyzed simulation results and verified them with available evidence.

5. OPERATIONAL AND PHYSICAL PARAMETERS

I used the most accurate available parameters and made conservative assumptions and simplifications to simulate flow through BOP components and the kinked riser. Although I understand that the fluid was composed of a mixture of liquid and gaseous hydrocarbons, my

[4] CFD is a numerical technique that solves fundamental equations of fluid motion using a computer-based iterative process.

model assumes that hydrocarbon flow can be approximated as a two-phase flow, *i.e.*, consisting of a single homogenous fluid phase,[5] carrying a dilute second phase of solid particles, which ultimately caused erosion. I made this assumption because accounting for an oil/gas/sand mixture flowing through a complex geometry would pose virtually insurmountable computational difficulties.[6]

I also made assumptions about sand production using information provided by Dr. Vaziri (see Appendix E). Specifically, I assumed a dilute particulate phase comprised of sand particles with a uniform size distribution (grains of sand 500 μm in diameter) and a concentration of 0.01 vol% (equivalent to approximately 100 lb/bbl). As set forth in Appendix E, Dr. Vaziri conservatively estimated a five-week duration of sand production and concluded that half the sand was likely produced in the first two weeks, by May 4, and the other half by the end of May.

In my simulations, I used bounding values to understand the sensitivity of the models to different flow rate conditions, with an upper bounding value of 0.01 m^3/s and a lower bounding value of 0.12 m^3/s, which are equivalent to production rates of approximately 5,000 and 65,000 bpd. I did not attempt to determine the actual or even likely flow rate, and these bounding values do not attempt to reflect such flow rates.

6. SIMULATION RESULTS

I completed three types of flow/erosion CFD simulations using Fluent:

- **Calibration simulations** of a model flow geometry to verify and calibrate the erosion model in Fluent;

[5] Specifically, I used a fluid mixture density range of ρ=645 - 688 kg/m^3 and viscosity range of ν=0.2 - 0.3 cP.

[6] For this reason, many multiphase flow simulators used in the oil and gas industry, such as OLGA™, make this same approximation.

- **Pre- and post-erosion simulations** of BOP components and the kinked riser; and
- **Transient simulations** of simplified BOP components.

6.1. Calibration Simulations

Before beginning complex simulations of BOP components, I tested and calibrated the erosion model in Fluent to ensure that the results would be accurate and meaningful. In that process, I applied the erosion model to a well-understood geometry of a pipe with a sudden restriction and expansion, carrying water with 2% sand, where reliable experimental flow and erosion data exist. (See Appendix C for details.) Based on the results of the calibration exercise, I fine-tuned the erosion model in Fluent to match the known experimental values. At this point, the Fluent package was ready for application to the BOP components and the kink in the riser.

6.2. Pre- and Post-Erosion Simulations

The critical BOP components and the kinked riser, recovered after the incident, had clearly been eroded, as illustrated in Figures 2 to 4.

To assess the effect, if any, of this erosion on flow rate, I set up two basic cases for each:

(i) the "**pre-erosion"** case, which refers to a component in its "intact" state and shape and in its position at the beginning of the simulated flow/erosion scenario, and

(ii) the "**post-erosion"** case, which refers to the state of the same element in which it was recovered—damaged by erosion.

For each case, I ran Fluent flow and erosion simulations to calculate change in pressure drop caused by erosion of each component. I then used these data to analyze the overall effect of erosion on flow rate. (See *infra*, Section 7.)

6.2.1. Simulations of the BSR

As noted, the BSR was activated April 22, but did not seal the wellbore as intended. Different parties have reported that the BSR did not seal the wellbore because the deformed drill pipe was held off-center (see Figure 5), and I relied on information provided by Nigel Richardson (see Appendix F) about the BSR standoff. Specifically, I used a gap of just under two inches between the blocks (see Figure 6), with the deformed drill pipe in between.

For approximately one week (April 22 - 29), hydrocarbons entered the BSR through the drill pipe and exited the partially sealed BSR by flowing through both the annulus and partially-severed drill pipe. Once the CSR was activated April 29, the flow path changed; hydrocarbons flowed up through and around the BSR in both the annulus and drill pipe.

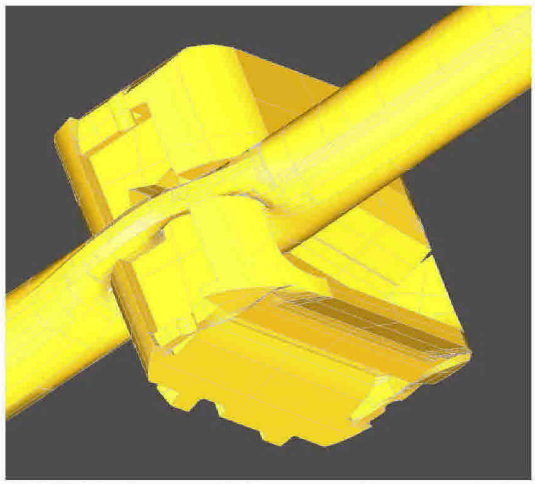

Figure 5. CAD models of BSR blades partially closed in on a deformed off-center drill pipe.

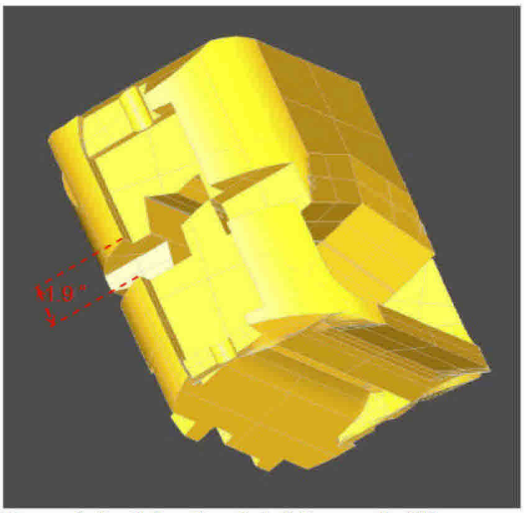

Figure 6. CAD model of the final 1.9" standoff between BSR blocks.

6.2.1.1. Pre-erosion CFD Simulations of the BSR

Erosion of the BSR began when the blocks partially closed April 22. To simulate the beginning of this process, I imported the pre-erosion BSR assembly internal flow geometry into Fluent and created a computational mesh. (See Appendix D for discussion of steps taken to create and import this geometry into Fluent.) I then ran fluid flow, particle tracking, and erosion simulations in Fluent.

The simulations reveal a complex flow path through the partially sealed BSR cavity, requiring hydrocarbon flow to traverse through a tight passageway on the sides of the partially closed blocks, increasing velocity (from one to 50 m/s) and creating turbulent flow conditions (see Figure 7 and Figure 8 below). The simulations also show that solid particles were swept up by the fluid and moved along similar trajectories, causing erosion, as shown in Figure 9.

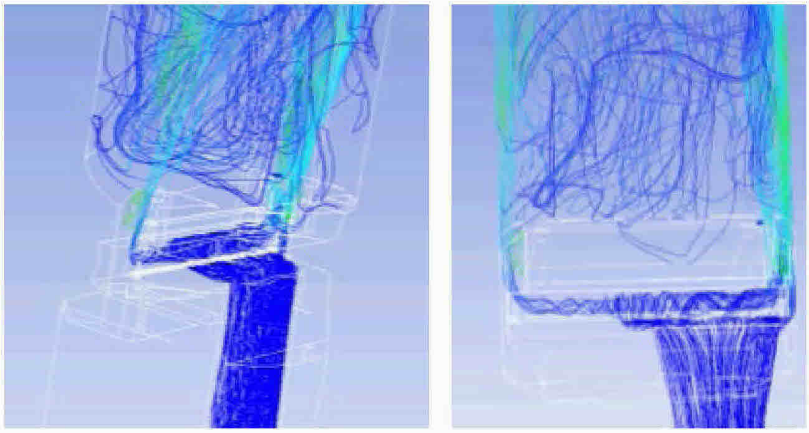

Figure 7. Pathlines of fluid passing through drill pipe and partially-sealed initial intact BSR assembly; lighter color indicates higher turbulence level.

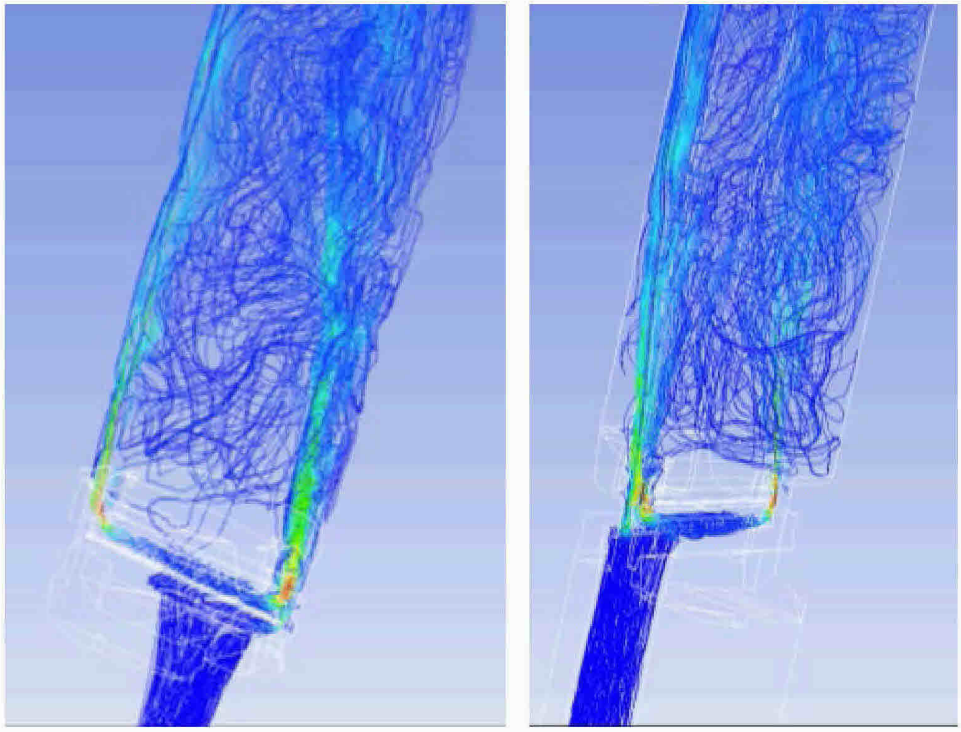

Figure 8. Pathlines of the fluid passing through partially sealed pre-erosion BSR assembly; red color indicates higher velocity.

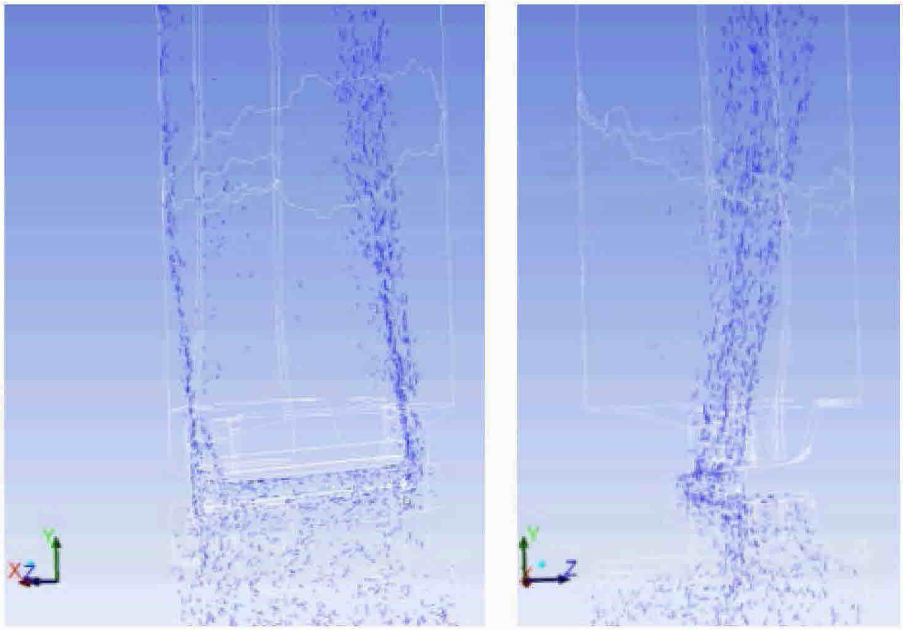

Figure 9. Solid particles passing through partially sealed pre-erosion intact BSR assembly.

The erosion simulations show that the most significant damage was along the sides of the BSR due to sudden changes of flow direction and high local velocity of the fluid, as seen in Figure 10 below.

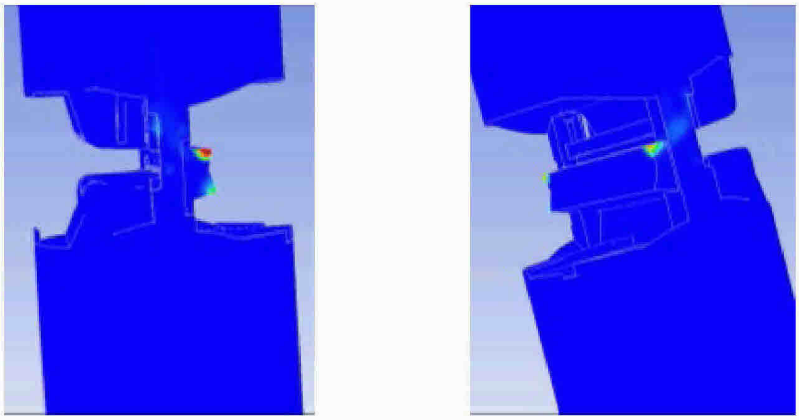

Figure 10. Erosion rate of pre-erosion BSR assembly; red color indicates high value.

After running Fluent flow and particle simulations, I compared the predicted erosion results with visual evidence of eroded BSR components. The Fluent-simulated erosion patterns

broadly agree with the recovered eroded BSR blocks—both when viewed by the naked eye and as laser scanned. The actual eroded blocks can be seen in Figure 2 above; the laser scan images are given below in Figure 11 and show that the most severe erosion occurred along the sides of the BSR blocks, consistent with Fluent simulations.

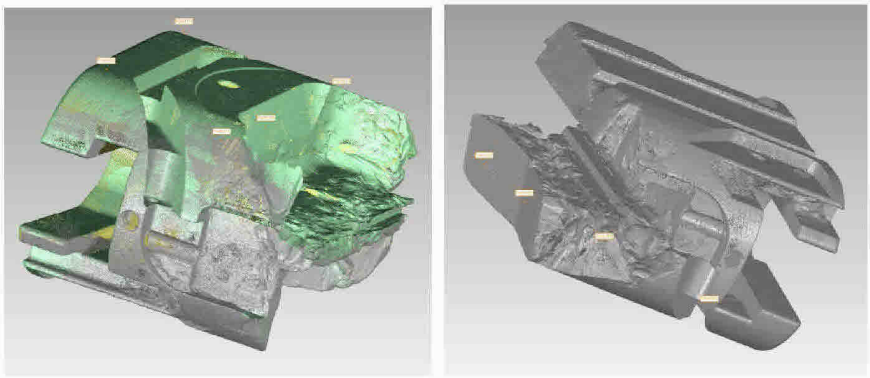

Figure 11. 3-D laser scans of the eroded BSR blocks.

6.2.1.2. Post-erosion simulations of the BSR

Next, I repeated the procedure of importing the eroded, laser-scanned BSR blocks and housing into Fluent and creating a mesh. (See Appendix D for details.)

Flow simulations of the post-erosion BSR assembly establish that erosion enlarged the flow path, allowing fluid and particles to pass more readily across the entire width of the blocks (see Figure 12). As erosion widened the flow path, maximum fluid velocity was reduced by four times compared to that of the pre-erosion case (assuming the same pressure drop). Particles followed the pathway of the fluid (see Figure 13). The erosion is spread out across the BSR blades, and at the point of maximum erosion, the rate is two orders of magnitude less than that of the pre-erosion blocks (see Figure 14).

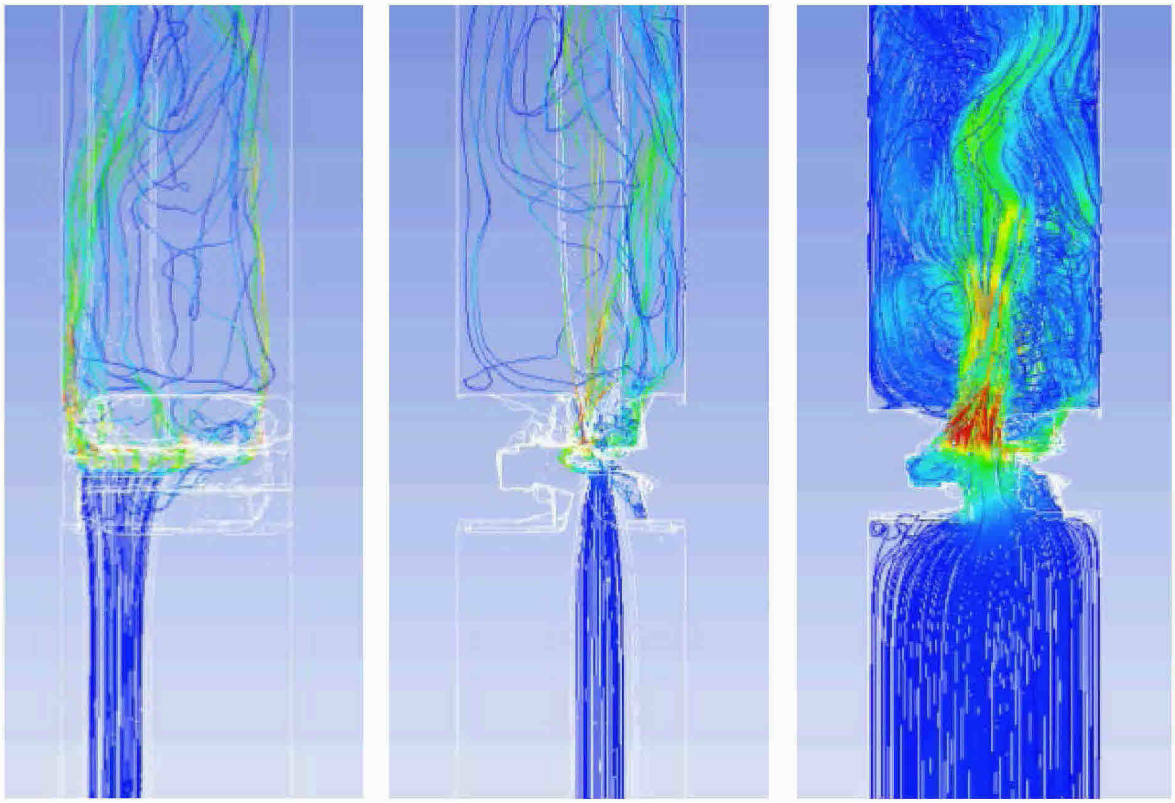

Figure 12. Pathlines of fluid passing through partially sealed post-erosion BSR assembly; red color indicates higher velocity.

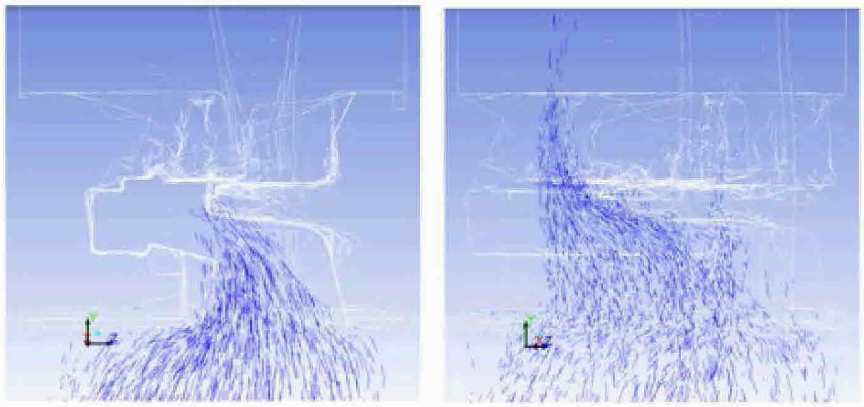

Figure 13. Solid particles passing through partially sealed post-erosion BSR assembly.

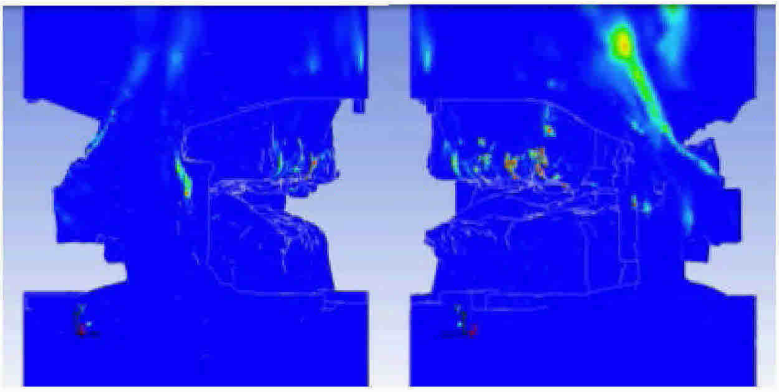

Figure 14. Predicted erosion of BSR assembly, red indicating high values.

6.2.2. Simulations of the CSR

After the CSR was activated April 29, hydrocarbons entered the CSR through the drill pipe and exited the CSR by flowing through both the annulus and severed drill pipe.[7]

6.2.2.1. Pre-erosion CFD Simulations of the CSR

Erosion of the CSR began when the blocks closed April 29 and lasted throughout the period of sand production, assumed to be May 27.

To simulate the beginning of this process, I modeled the initial flow geometry and ran fluid flow, particle tracking, and erosion simulations. I set up the pre-erosion CSR flow geometry using the same steps described above for the BSR and created a computational mesh (shown in greater detail in Appendix D).

The simulations depict a flow path between the central parts of the CSR blades, causing fluid velocity to increase substantially (see Figure 15a). As shown below in Figure 15b, solid particles were swept up by the fluid and moved along similar trajectories, causing erosion. The

[7] Based on photographic evidence showing minor erosion of the VBRs, there appears to have been some flow through the annular space below the CSR. However, there was at least a partial metal-on-metal seal at the VBRs and the fraction of the overall flow coming through the annulus remained small. Therefore, I consider it appropriate not to include this flow path in my analysis.

most significant erosion rate is seen in the middle section of the CSR blocks, where the solid particles impacted upon exiting the drill pipe (Figure 16).

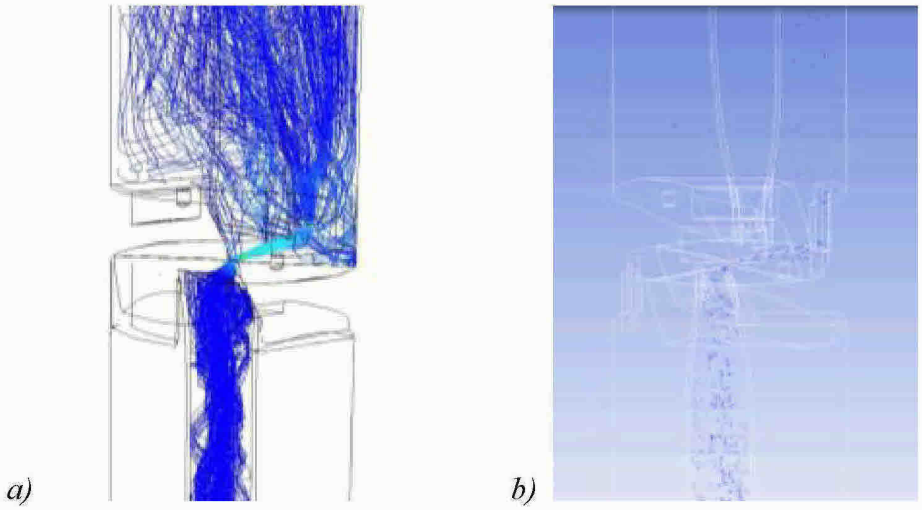

Figure 15. a) Pathlines of fluid and b) solid particles passing through drill pipe and pre-erosion CSR assembly; lighter color indicates higher velocity.

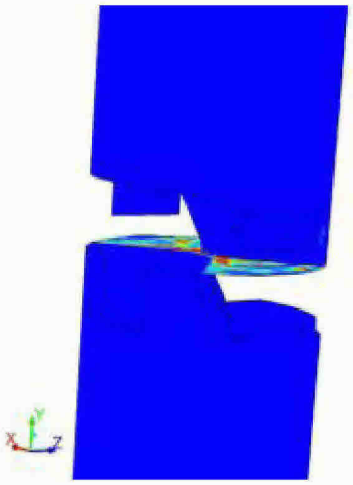

Figure 16. Erosion rate of pre-erosion CSR assembly; red indicating high values.

As with the BSR, the Fluent-simulated erosion patterns broadly agree with the recovered CSR blocks - based on visual inspection and laser-scanned images. The actual eroded blocks can be seen in Figure 3 above; the laser scan images are given below in Figure 17 and show that the

most severe erosion occurred in the center of the blades, consistent with Fluent simulation results.

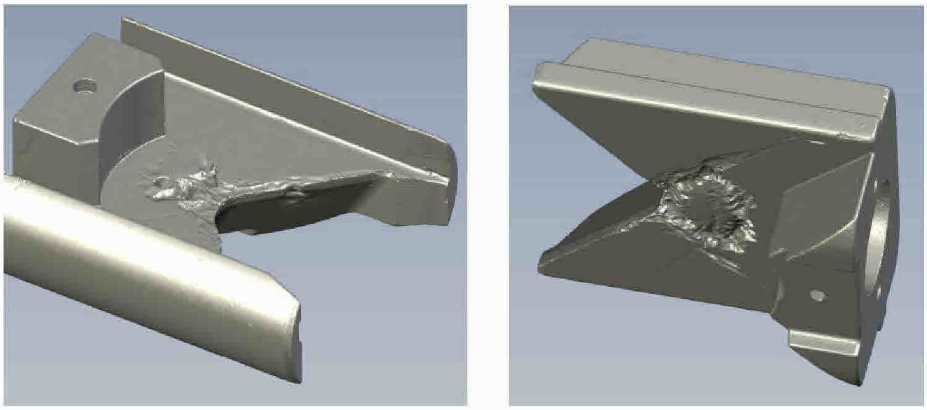

Figure 17. Laser scans of eroded CSR blocks.

6.2.2.2. Post-erosion CFD Simulations of the CSR

Next, I repeated the process of importing the eroded, laser-scanned CSR block assembly into Fluent, creating a mesh and performing simulations. (See Appendix D for details.)

The CFD simulations for the post-erosion CSR blocks establish that erosion widened the flow path between the CSR blades (see Figure 18a), making it easier for fluid to pass between blocks. The simulations reveal that particles continued to pass through the gap in the middle of the eroded CSR blocks (see Figure 18b), primarily damaging the central section of the CSR blocks (see Figure 19).

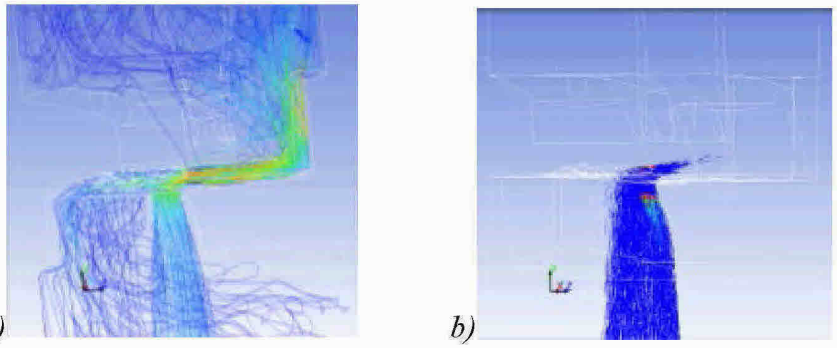

Figure 18. a) Pathlines of fluid and b) solid particles passing through drill pipe and eroded CSR assembly; red indicates higher velocity and higher erosion rate.

Figure 19. Erosion rate of eroded BSR assembly; red color indicates high values.

6.2.3. Simulations of the UAP

Because the exact UAP flow geometry was not available (in either the pre-erosion or post-erosion state), I constructed a simplified flow geometry of the UAP for simulations. Other parties have already established that the section of the drillpipe passing through the UAP failed rapidly in the days following the incident and was pushed into the riser, together with the severed section of the drill pipe below it. Therefore, the UAP flow geometry that needed to be simulated here consisted of sudden constriction of the wellbore followed by sudden expansion.

Although it is clear from the recovered elements of the UAP that the original elastomer was completely eroded along with the edges of the UAP "fingers," this erosion did not lead to a

significant change of the flow pattern and pressure drop through the UAP. This minimal impact is confirmed by transient flow and erosion simulations, described below.

6.2.4. Simulations of the Kinked Riser

When the *Deepwater Horizon* rig sank, it caused the base of the riser to form an approximately 90-degree kink and, with the kink, created another flow restriction (see Figure 20). On April 28, two holes are seen in the kink which have likely been formed by erosion. A third hole appeared May 19, and is depicted in Figure 21. The three holes which formed first (shown in Figure 21) bear classic indications of erosion.

Three additional holes were found on the recovered section of the kink in the riser, as indicated in Figure 22. The additional holes which appeared later on the side of the kink in the riser are likely a consequence of intense mechanical deformation leading to cracking at these locations. Signs of erosion around these additional holes suggest that some sand production continued after they were formed. Each of the holes was enlarged in size over time due to erosion.

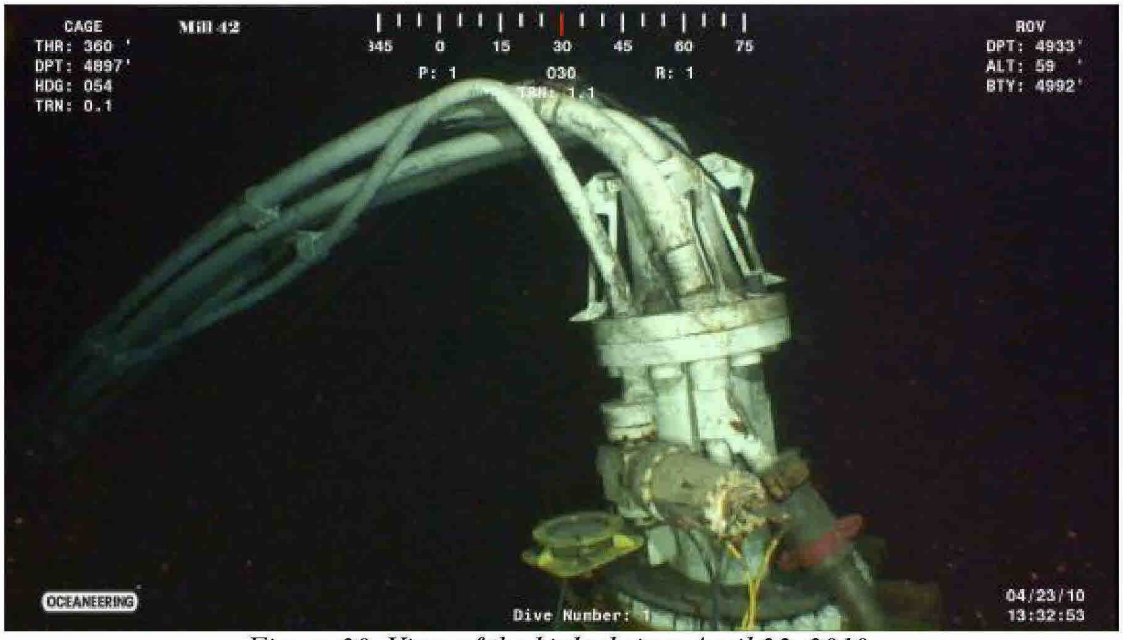

Figure 20. View of the kinked riser April 23, 2010.

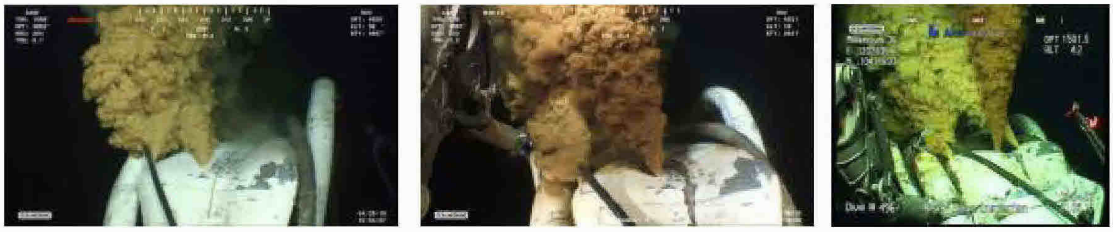

Figure 21. Images of first three holes in the kinked riser taken on April 28, May 4, and May 21, 2010 (left to right).

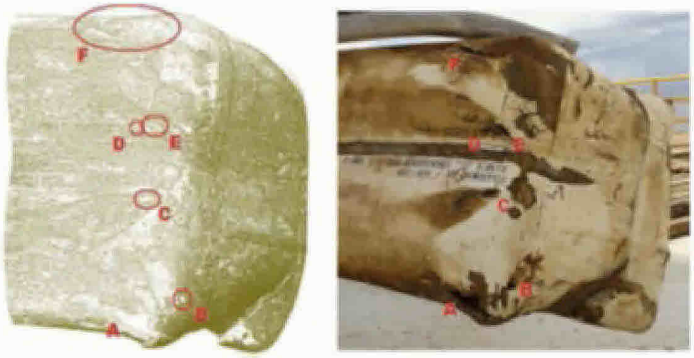

Figure 22. Laser scanned image and photo of kink showing location of six holes, annotated A through F.

6.2.4.1. Pre-erosion CFD Simulations of the Kinked Riser

Erosion of the kinked riser began April 22, when the *Deepwater Horizon* rig sank, and lasted throughout sand production, assumed to be May 27. To simulate this process, I modeled the initial flow geometry and then ran fluid flow, particle tracking, and erosion simulations. The actual parts of the dismembered kinked riser were laser scanned, reassembled, and converted into a CAD model (Figure 23) and then imported into Fluent and meshed.[8]

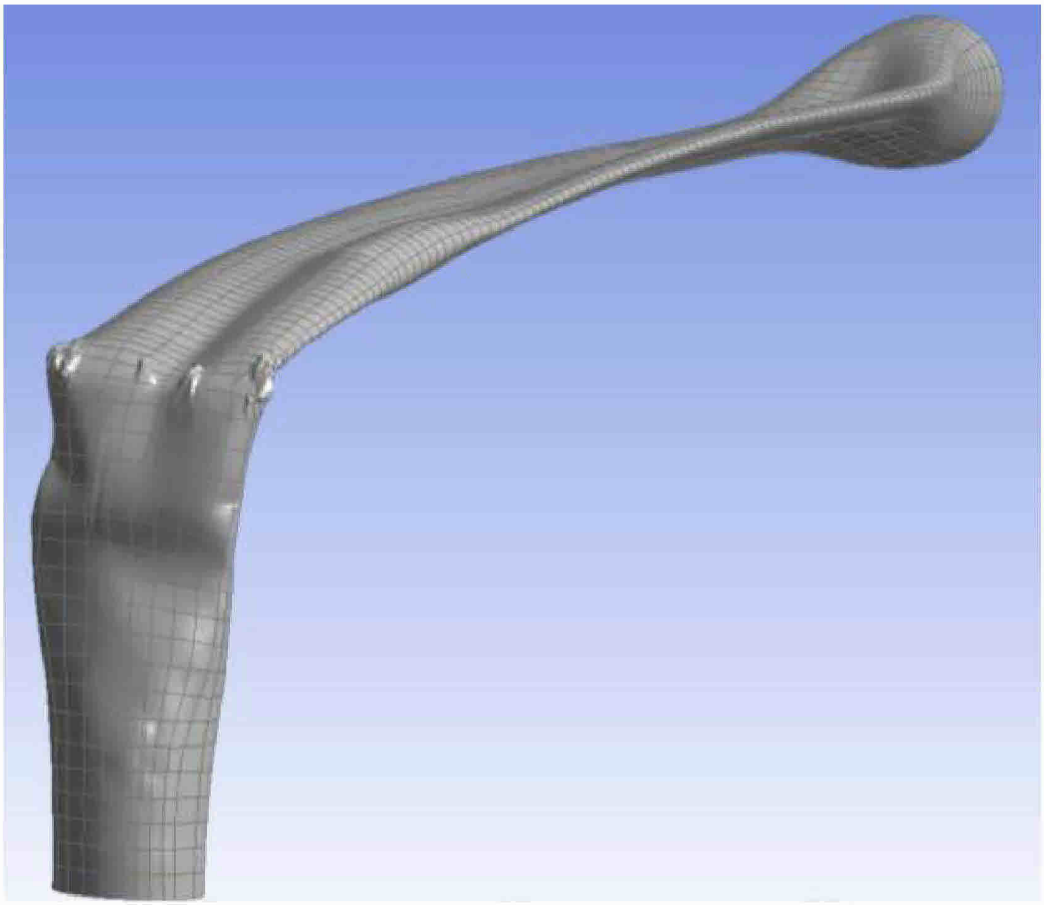

Figure 23. CAD model of the pre-erosion kinked riser flow geometry.

The simulations show that fluid accelerated up to 50 times as it passed through the narrow, dog-bone shaped, cross-section of the kink, see Figure 24, and that solid particles

[8] The two pieces of severed drill pipe trapped inside of the kink are not included in this analysis.

passing along that same flow path eroded parts of the kinked riser (see Figure 25 and Figure 26). Again, the Fluent simulation results agree with the actual location of holes in the recovered kink (see Figure 22, above).

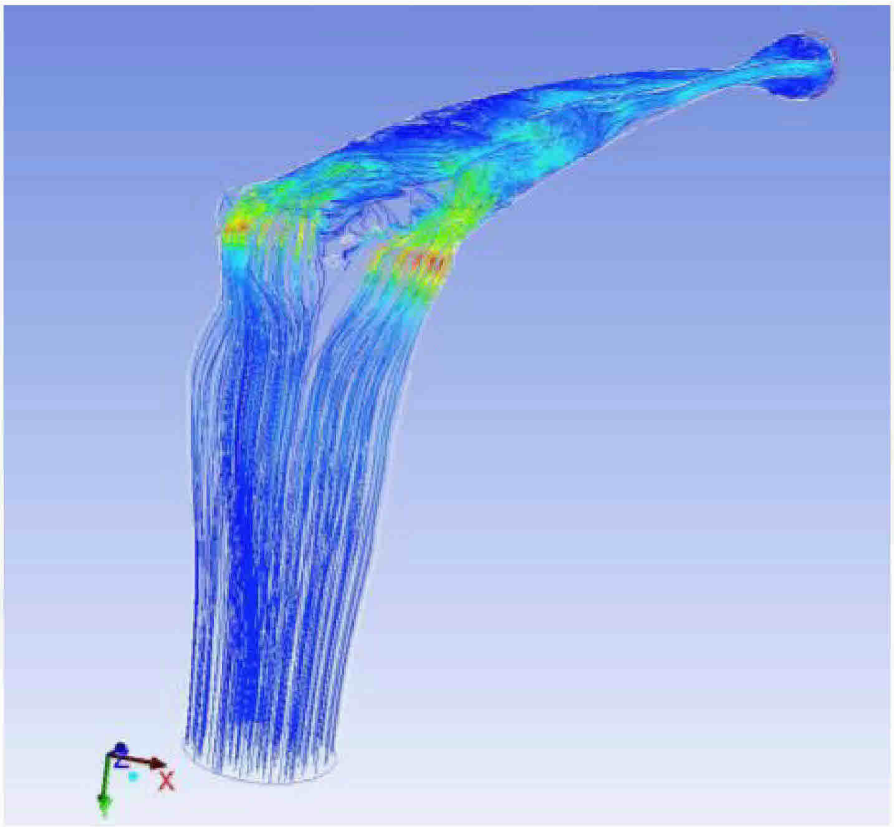

Figure 24. Pathlines of fluid passing through pre-erosion kinked riser; red color indicates higher velocity.

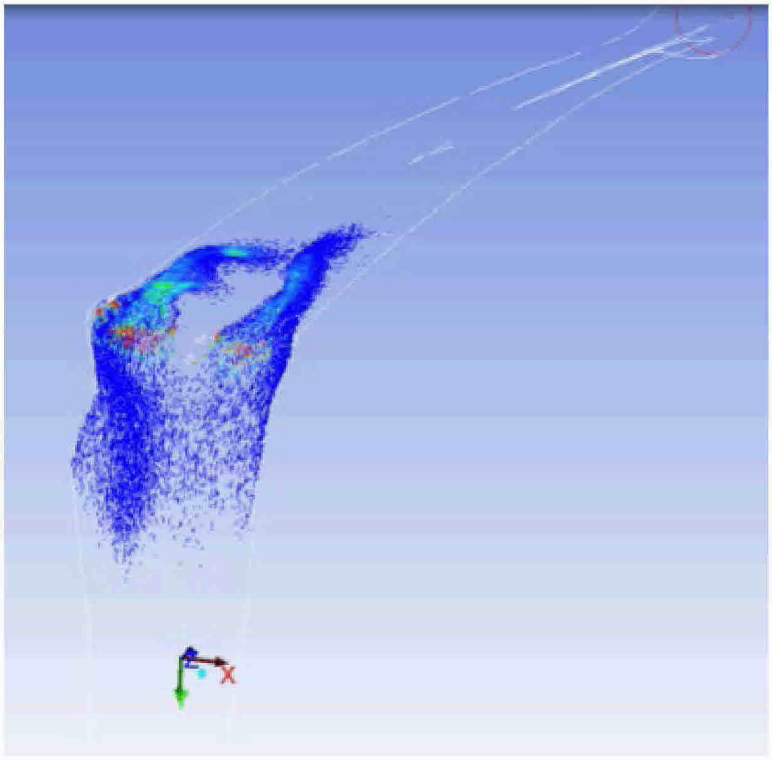

Figure 25. Solid particles passing through pre-erosion kinked riser, colored by erosion intensity.

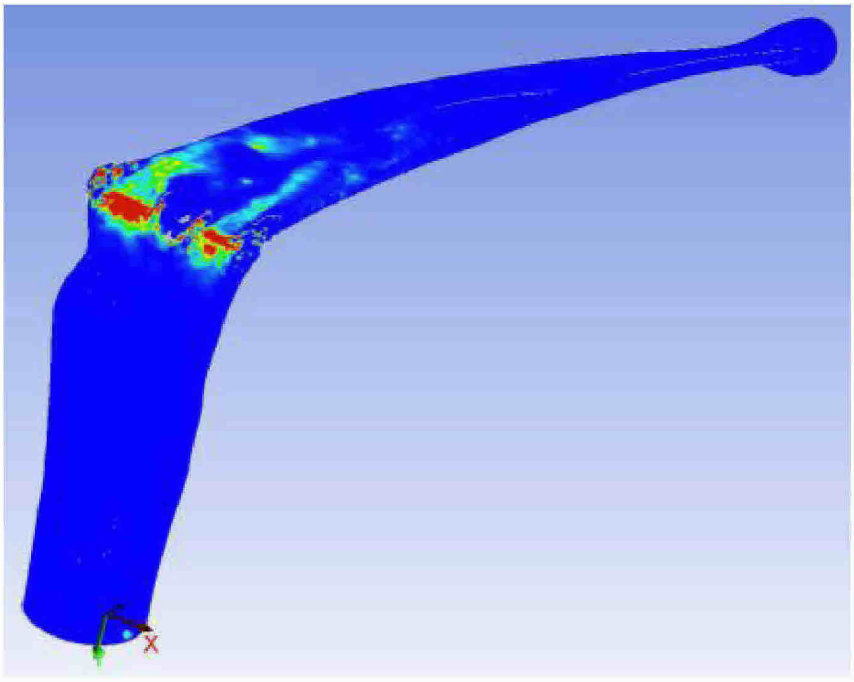

Figure 26. Predicted erosion of pre-erosion kinked riser, red indicating high values.

6.2.4.2. Post-erosion CFD Simulations of the Kinked Riser

For the post-erosion simulation of the kinked riser, I introduced three holes into the wall of the pipe following the kink (see Figure 27). I approximated the location based on:

a) the appearance of holes and the leaks in the recovered kink shown in Figure 21,

b) the laser scans and photo shown in Figure 22, and

c) the predicted locations of maximum erosion shown in Figure 26.

In my analysis, the three holes (B, C, and E in Figure 22)[9] have the following geometry:

- Hole B: cross sectional area: 113 mm^2, perimeter: 38 mm;
- Hole C: cross sectional area: 178 mm^2, perimeter: 69 mm;
- Hole E: cross sectional area: 178 mm^2, perimeter: 69 mm.

To simulate the backpressure effect provided by the remainder of the riser lying on the ocean floor, I assumed pressure at the exit of the kinked riser to be 300 psi higher than at the exit of the holes.

The simulations establish that approximately 22% of the flow exited through the three holes at the kink, with the remaining 78% traveling through the end of the riser (see Figure 28). Erosion continued at the same locations, and the erosion rates remained high (see Figure 29), suggesting a steady erosion process throughout the period of sand production.

[9] I considered that holes D and E led to a single, combined leak.

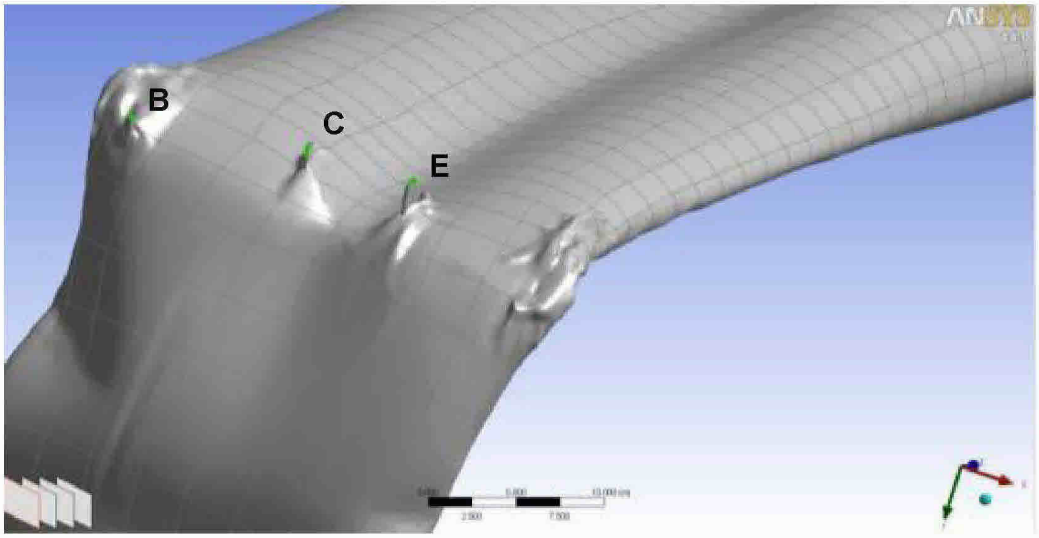

Figure 27. CAD model of post-erosion kinked riser flow geometry with three holes (B, C and E).

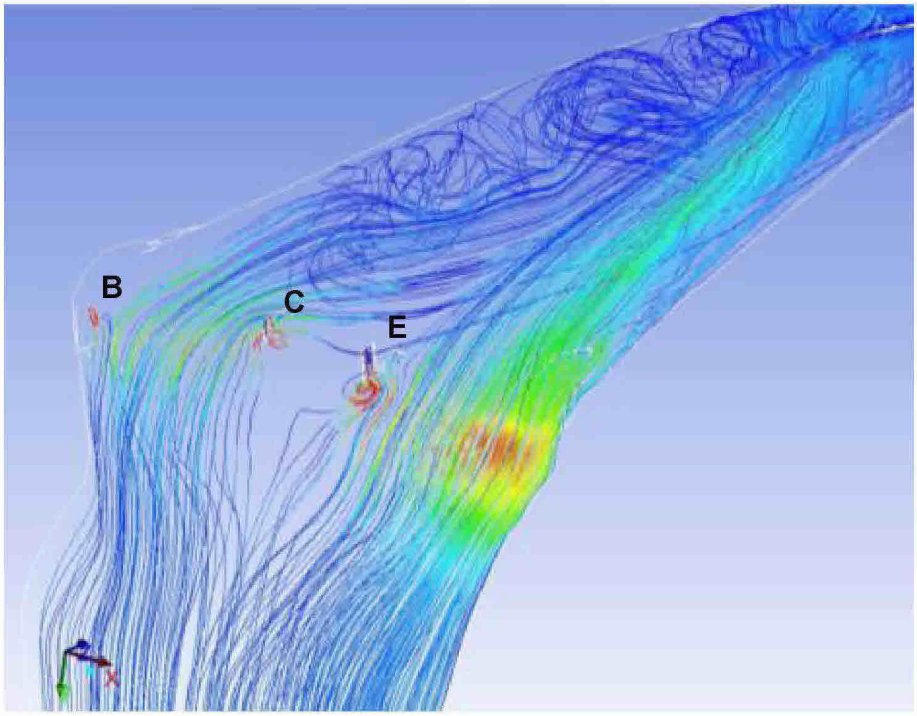

Figure 28. Pathlines of fluid passing through post-erosion kinked riser; red color indicates higher velocity.

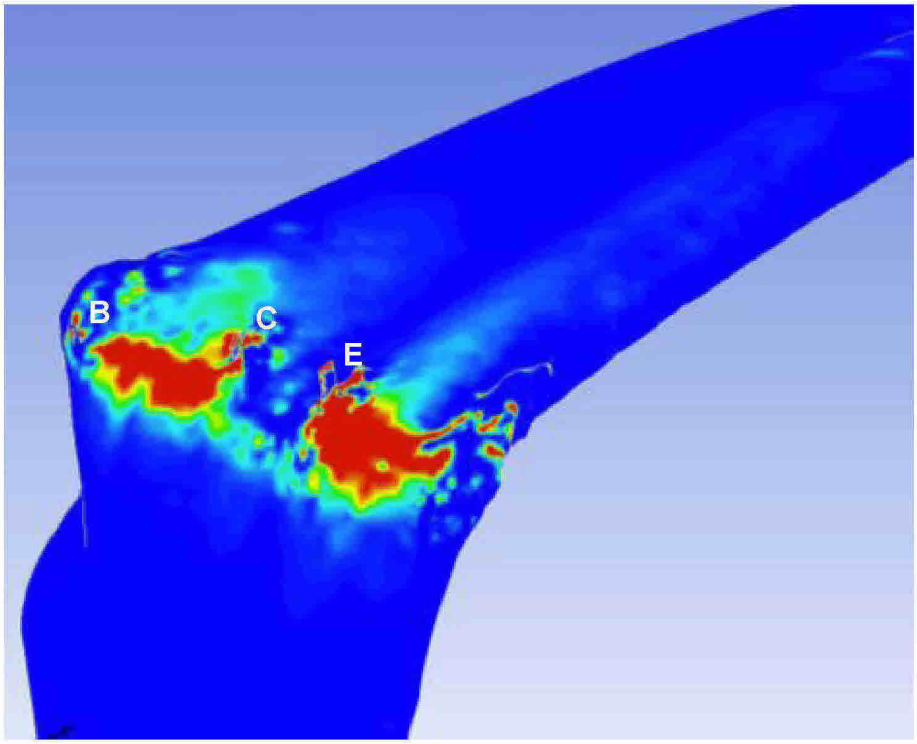

Figure 29. Predicted erosion of the post-erosion kinked riser, red indicating high values.

6.3. Transient Simulations of the BOP Elements

The pre- and post-erosion simulations discussed above capture two points in time—the beginning and end of the erosion process. In other words, the simulations establish the flow restriction provided by each component at the beginning and end of erosion.

To flesh out the erosion process between these two times, I recreated simplified versions of the BSR and CSR and then performed transient CFD simulations. The simplified versions of the BOP components retained all key features important for CFD simulations of these elements, but omitted unnecessary geometrical details that complicate and lengthen the simulations.

Figure 30, which represents a simplified BSR flow geometry, is a good example. The resulting flow pattern (see Figure 31) is in broad agreement with the flow pattern obtained for the actual BSR geometry (Figure 8). One can see that the main feature of the flow—its motion "sideways" to pass through the constricted space—is retained.

Consequently, I was able to assume that the key features related to the dynamics of erosion and the resulting change in flow geometry of the BOP elements could be captured using transient CFD simulations of the simplified geometries. Using this approach, I established how erosion and change of flow geometry over time affected pressure through BOP components.

For all the simulated geometries (BSR, CSR and UAP), I obtained a linear change of pressure over time.

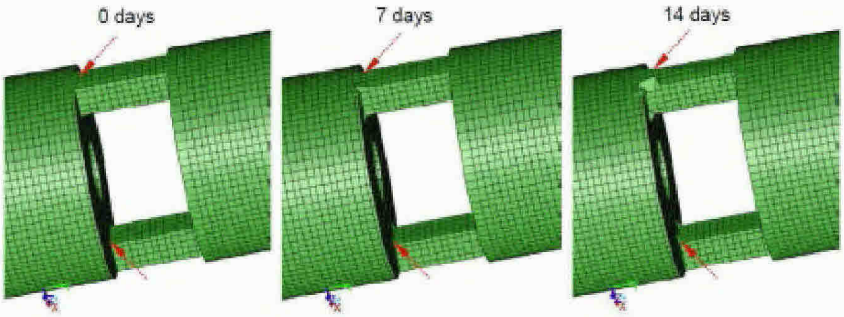

Figure 30. Transient simulation showing erosion of BSR flow geometry; red arrow points to locations of maximum erosion.

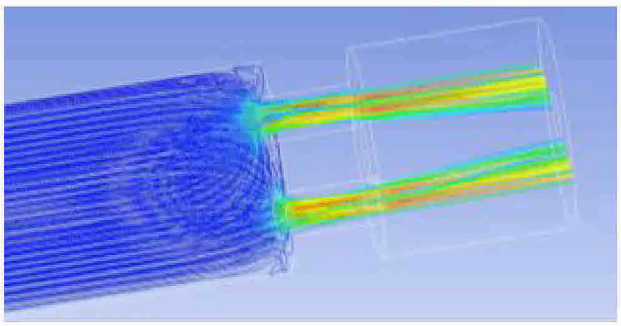

Figure 31. Pathlines of fluid passing through BSR assembly; red color indicates higher velocity

7. ANALYSIS AND DISCUSSION

After I completed the simulations presented above, I estimated change of flow rate through the eroded BOP and kinked riser. It bears emphasis that while executing the work, I did not know *a priori* the magnitude of the flow rate, so I did all simulations twice, using arbitrary

"bounding" values: a low estimate of flow rate at 5,000 bpd and a high estimate of flow rate at 65,000 bpd. My main goal was to estimate how any given flow rate (high or low) *changed* as elements of the BOP and kinked riser eroded.

To evaluate this change, I focused on pressure drop, the best indicator of resistance to flow. Therefore, I calculated pressure drop for each component for a given flow rate and then evaluated how it changed over time due to erosion and the resulting change of flow geometry.

Although the analysis of the components of the BOP and kinked riser was done separately for each element, to get a true picture of the overall effect of erosion on flow rate, I considered the overall assembly. This approach is necessary as the flow rate at any point is determined by overall resistance in its path, which is obtained as the sum of resistances of elements in series. In other words, to determine the effect on flow rate, I needed to look at the overall sum of pressure drops along the BOP elements and kinked riser and how that total changed due to erosion (for an illustration see Figure 32).[10]

Once I determined the pressure drop created by each component using CFD, I combined individual pressure drops to determine cumulative pressure drop across the system:

$$\Delta p = \Delta p_{CSR} + \Delta p_{BSR} + \Delta p_{UA} + \Delta p_{KR}$$

[10] Although I did not consider other resistances to flow, such as those in the well and collapsed riser, or the change of pressure in the reservoir, my analysis accurately describes change in resistance to flow due to erosion of the BOP and kinked riser.

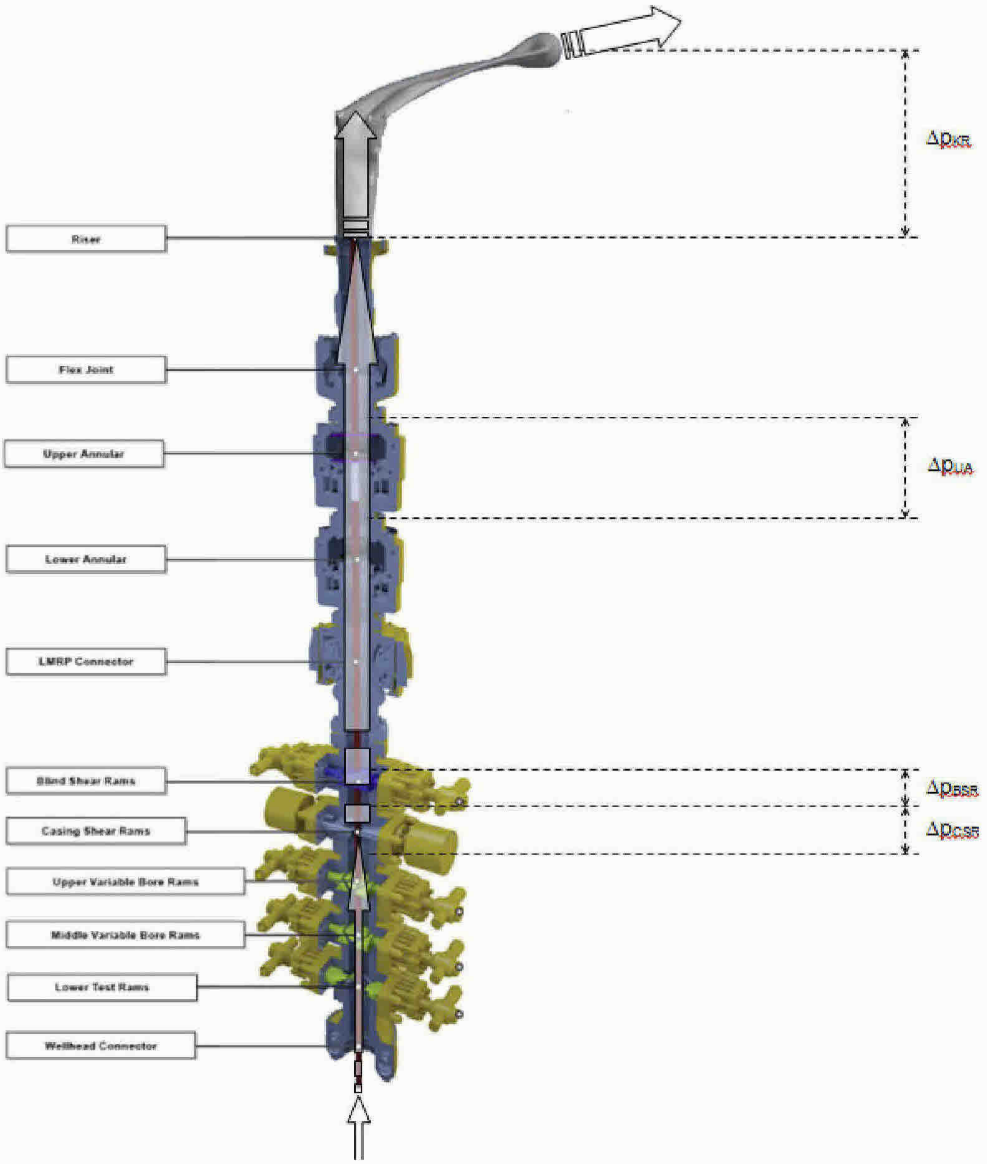

Figure 32. Cutaway view of Deepwater Horizon *BOP stack and superimposed riser kink with associated fluid path and the most significant pressure drop locations, from April 22-May 27, 2010*

Because the pressure drops of each component changed over time due to erosion, Figure 33, shown below, depicts calculated time evolution of the overall pressure drop, Δp, for the system as well as that contributed by each component. I show a relative[11] change of pressure drop as a function of time because I was able to prove that this normalized change of pressure drop was a "universal" feature of the flow/erosion process, *i.e.* it was the same (within 2-3%) for the entire range of flow rates considered, from 5,000 to 65,000 bpd. Therefore it is safe to assume that the trend in Figure 33 is universal for the range of conditions I considered, irrespective of actual flow rate.

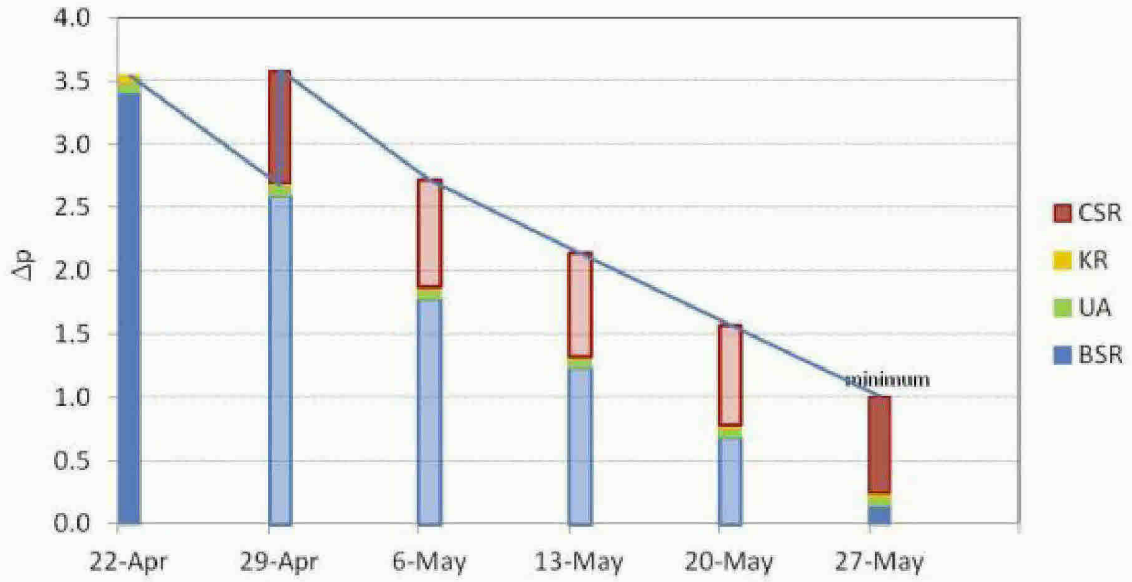

Figure 33. Normalized change in pressure drop seen for individual components and the cumulative change in the overall pressure drop, April 22- May 27, 2010.

The simulations establish that the dominant resistance to flow (pressure drop) was initially created by the BSR (as seen in Figure 33). Specifically, the BSR pressure drop

[11] I used the pressure drop on May 27 to normalize all other values in Figure 33.

represents 96% of total pressure drop on April 22, which decreased due to erosion to 72% by April 29 when the CSR was activated and to just 15% by May 27.

When the CSR was activated April 29, it temporarily increased the overall resistance to flow (pressure drop). The CSR accounted for approximately 25% of the pressure drop in the beginning, and by the end it was the dominant resistant to flow: 76% of the total. The UAP and kinked riser (KR) contributed less resistance to flow at all times.

The pressure drop numbers at the beginning and end of the simulated period represent "hard" numbers because the exact flow geometries are known, whereas I interpolated the values between those two points using transient CFD simulations of BOP geometries (discussed in Section 6.3).[12]

The effects of erosion on the BOP components and kinked riser on flow rate are reflected in the pressure drop results. According to CFD simulations and consistent with the trend depicted in Figure 33, pressure drop across the BSR decreased due to erosion by a factor of 23 over the five-week period. The pressure drop across the CSR decreased by only approximately 15% in the four weeks after they were activated, which explains why by the end of sand production (assumed to be May 27), the CSR was the largest flow restriction in the system. The joint contribution of the UAP and kinked riser to overall pressure drop remained relatively small and did not change much in this period, increasing from 3.6% on April 22 to 9.2% on May 27.

Pressure drop is directly related to flow rate. I used a well-established quadratic relationship for single-phase flow between pressure drop and flow rate: $\Delta p \sim Q^2$, to estimate

[12] In Figure 33 and Figure 34, the darker colored bars represent "hard" numbers obtained by CFD simulations of the real BOP components, while the lighter colored bars represent interpolated numbers, obtained from transient CFD simulations of geometries.

change in flow rate due to erosion of the BOP components and kinked riser, as presented in Figure 34.[13]

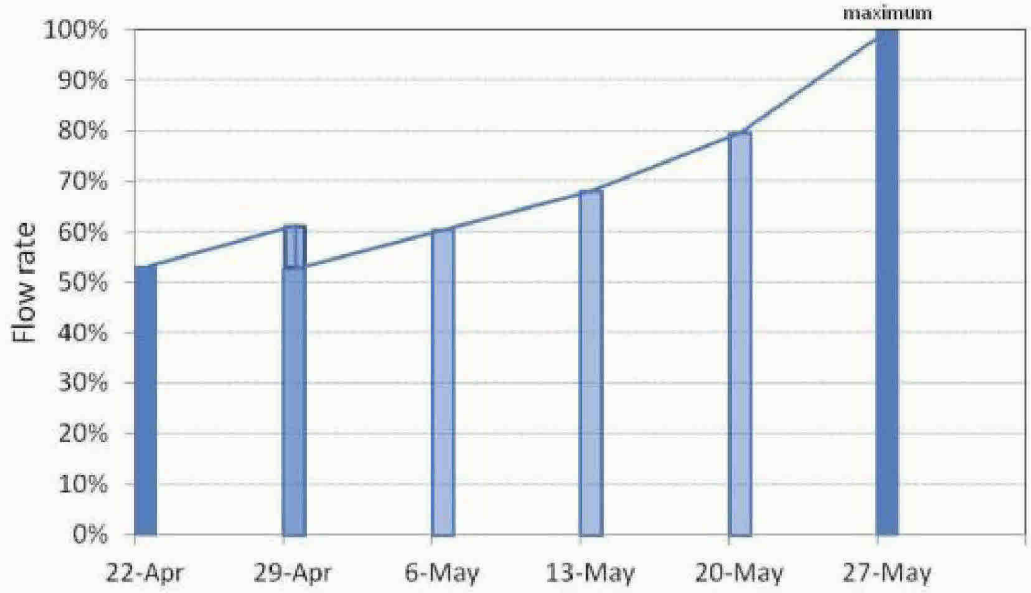

Figure 34. Normalized change in flow rate during assumed period of erosion, April 22 - May 27, 2010.

Assuming the BOP and kinked riser were the main restrictions to flow in this period, Figure 34 shows that flow rate would have almost doubled (increased by 88%) over the first five weeks of the incident due to erosion (assuming a sanding end date of May 27). This relative change of flow rate is virtually the same (within ± 2%) regardless of whether flow is assumed to be 5,000 or 65,000 bpd or any value in between.

8. RESPONSE TO OTHER EXPERT OPINIONS ABOUT EFFECTS OF EROSION ON FLOW RATE

I have reviewed three expert reports provided to me that address or discuss, in part, the effect of erosion on flow rates:

[13] In Figure 34 the flow rate data are normalized – presented relative to maximum flow rate on May 27.

" Flow Rates from the Macondo MC252 Well," by Ronald C. Dykhuizen.

"Oil Release from the MC252 Macondo Well," by Stewart K. Griffiths, and

"Estimate of Cumulative Volume of Oil Released from the MC252 Macondo Well," by Mehran Pooladi-Darvish

With respect to all three reports, I focused primarily, if not exclusively, on those portions that discuss erosion. As a general matter, all three cover erosion superficially and conclude, without meaningful analysis, that erosion did not significantly affect flow rates at Macondo. Perhaps most fundamentally, all three reports base their flow calculations on data available in the latter stages of the incident (toward the end of the flow period, when more data were available) and then make arbitrary assumptions about what happened in the first few weeks following the blowout. Indeed they all ignore hard evidence of erosion occurring well after the first few days following the blowout, including erosion of the CSR, which did not even close until April 29, and ROV footage of the kinked riser, which indicates erosion well into May.

Pooladi-Darvish Analysis

Although his report is the most detailed of the three in terms of seeking to determine the effects of erosion in the weeks following the blowout, Dr. Pooladi-Darvish fails to make a convincing case about what actually happened to the restrictions to flow within the BOP during the first five weeks (April 22 - May 27), when only a few BOP pressure measurements were available (none before May 8), making it difficult to calibrate his models.

Dr. Pooladi-Darvish states (on page 24, paragraph 4) that:

"…the BOP restriction did not change significantly after May 8, 2010. However, one could imagine a case where during the early days of the blow out, the BOP would have exerted more restriction against flow, but soon eroded away. There is no BOP pressure data available during those early days to confirm whether this erosion led to a significant change in the BOP restriction,"

(emphasis added) There is no need to *imagine* that the BOP initially restricted flow, and that the restriction then decreased due to erosion. My models and analysis directly demonstrate such an effect, and I have also quantified the effect of erosion on flow rate and provided a timeframe over which it happened.

Even if there were no pressure data before May 8, the ones set forth in Figure 16 of the Pooladi-Darvish report show a rapid decrease in BOP pressure in the first half of May, which is consistent with my findings about erosion of BOP components. This rate of pressure decrease is more rapid than that in June and July, after most erosion had occurred.

Therefore, I tend to agree, and only broadly, with only the first of the four initial flow scenarios offered by Dr. Pooladi-Darvish, *i.e.* with the so-called "Restricted BOP" scenario. Under this scenario, which Dr. Pooladi-Darvish calls "extreme," there was no flow immediately following the blowout when the BSR closed, and then, because of erosion, pressure drop through the BOP linearly decreased and flow increased until May 8. Based on my own analysis, this scenario is neither extreme nor ill-founded. Rather, it proves to be realistic with two obvious corrections -- to account (i) for flow at the beginning (which caused erosion in the first place) and (ii) for flow rate to continue to increase throughout May, as both my analysis and pressure data support.

Griffiths Analysis

Dr. Griffiths's report offers arbitrary, unfounded, and incorrect statements about the role of erosion on flow rate. As just one example, Dr. Griffiths writes on page 47, paragraph 2:

> "Upon recovery, the BSR showed very extensive erosion on the sides and under side of the recess, but I do not believe that this erosion significantly reduced the pressure drop across the ram. Instead, I believe that the initial openings were sufficiently large that the pressure drop measured later in May was comparable to that present from its first closure."

This statement is clearly incorrect given that precise CFD simulations which I have conducted show that pressure drop across the BSR decreased by a factor of 23 due to erosion.

Indeed, Dr. Griffiths's opinions on erosion are so arbitrary that they conflict with one another. For example, Dr. Griffiths writes on page 46, paragraphs 2 and 3:

> "Each of these rams was closed with the intent to further restrict the BOP and so reduce the flow rate of oil. As such, I might reasonably assume that flow rates from the well *decreased* continuously up to May 8 in response to each subsequent closure of a ram. In this case, flow rates before May 8 would be at least as large as my calculated rate based on the first measured BOP pressures. . . Assuming that flow rates decreased permanently in response to each ram closure does not, however, take into account the possibility of erosion in the rams or captured pipe between the time a ram was activated and the later date of May 8. Such erosion can occur very rapidly when fluid speeds are large, so flow rates may well have *increased by* May 8 from their values at the time a ram was first closed."

(emphasis added.) In other words, Dr. Griffiths first states that flow rate "*decreased* continuously up to May 8 in response to each subsequent closure of a ram," which is not correct as flow rates responded virtually instantaneously when rams closed, and then asserts precisely the opposite in the following statement that "such erosion can occur very rapidly when fluid speeds are large, so flow rates may well have *increased* by May 8 from their values at the time a ram was first closed."

Likewise, I disagree with Dr. Griffiths's analysis of the eroded kinked riser. Specifically, Dr. Griffiths writes on page 47, paragraph 3:

> "My inspection of the recovered riser showed little erosion in the kink, except in the vicinity of the several leaks. These leaks clearly originated from cracks that formed due to folding of the riser that were subsequently enlarged by erosion. There was extensive erosion downstream of each leak indicating very significant flow beyond them."

These conclusions are contradicted by my own visual inspection of the same sections and the CFD simulations I performed to model locations and rates of erosion in the kinked riser. Although some breaches of the pipe wall on the sides of the kink may have originated by

cracking, at least two of the three main holes were clearly formed in areas where stress and strain of the pipe wall were not as high and would not have led to cracks. Furthermore, the shape of the metal surface around and within the holes I observed as well as the absence of significant damage to the pipe wall away from them are clear signs of erosion damage.

Finally, Dr. Griffiths's summarizes on page 11, paragraph 1:

> "…any erosion in the BOP that affected flow rates therefore had to occur over the first few days such that the state of the BOP over the great majority of the 86 days was comparable to that at shut-in on July 15."

This statement lacks any support and in fact is conclusively disproven by my work.

Dykhuizen Analysis

Finally, Dr. Dykhuizen does not even attempt to discuss effects of BOP erosion on flow rate. Rather, he dismisses its importance outright, without proof and by citing Dr. Griffiths's flawed analysis, discussed above.

Although Dr. Dykhuizen is correct that "the steady decline in the BOP pressure is consistent with depletion of the reservoir," it does not follow that "erosion was not an important factor." (Report at p. 10). To the contrary, erosion of the BOP led to a decline in BOP pressure and the two effects cannot be separated without an analysis of the type I conducted.

Srdjan Nesic, Ph.D

APPENDIX A: CURRICULUM VITAE

SRDJAN NESIC

Russ Professor of Chemical Engineering
Director, Institute for Corrosion and
Multiphase Flow Technology
Ohio University
Athens, OH 45701,
USA

tel: + 1 (740) 593 9945
fax: + 1 (740) 593 9949
email: nesic@ohio.edu
http://www.corrosioncenter.ohiou.edu/nesic/
http://www.corrosioncenter.org

EDUCATION

Ph.D. 1991 University of Saskatchewan, Canada, Department of Chemical Engineering.
M.Sc. 1988 University of Belgrade, Yugoslavia, Department of Mechanical Engineering.
B.Sc. 1982 University of Belgrade, Yugoslavia, Department of Mechanical Engineering.

WORK

2002 – present Professor of Chemical Engineering and Director of the Institute for Corrosion and Multiphase Flow Technology, Ohio University, Athens, Ohio, USA.
1996 – 2001 Senior Lecturer, Department of Mechanical Engineering, University of Queensland, Brisbane, Australia.
1991 – 1996 Principal Research Scientist, Institute for Energy Technology, Kjeller, Norway.
1994 – 1995 Part time lecturer at the University of Oslo, Norway.
1983 – 1988 Research Scientist, Vincha Institute for Nuclear Sciences, Belgrade, Yugoslavia.

2009, 2010 Visiting Professor, Department of Physical Chemistry and Electrochemistry, Faculty of Technology, University of Belgrade, Belgrade, Serbia.
2008 Adjunct Professor, Department of Applied Chemistry, Curtin University of Technology, Perth, Australia.
2006 Visiting Professor, Department of Physical Chemistry and Electrochemistry, University of Milan, Italy
2003 – present Editorial Board, Corrosion Journal (NACE International), SPE Journal (Society of Petroleum Engineers).

HONORS

2012 Appointed member of National Academy of Sciences (NAS) committee investigating pipeline transportation of diluted bitumen
2011 Appointed Russ Professor of Chemical and Biomolecular Engineering at Ohio University
2010 Received award for best paper published in the Corrosion Journal (NACE International) in 2011
2008 Appointed as Fellow of NACE International, Houston
2007 Received H.H. Uhlig Award for outstanding effectiveness in post-secondary corrosion education, NACE International, Houston

2006	Nominated to Serbian Academy of Sciences and Arts
2002	Appointed Honorary Research Fellow, School of Engineering, University of Queensland Brisbane, Australia
2001	Received 1st prize, Best Tertiary Educational Website, Australian Publishing Association Awards
1998	Received Bengough award by the Institute of Materials for research paper in British Corrosion Journal, UK.

PUBLICATIONS

10+	Book articles
70+	Peer reviewed papers in reputable international journals and monographs
100+	International conference papers
50+	Scientific reports

OTHER

10+ times	Served as session or symposium chair at the annual NACE International Conferences, and other international conferences,
10+ times	Delivered keynote, plenary and invited lectures, at various international conferences,
15+ times	Worked as consultant/advisor on corrosion related projects for the oil and gas industry,
4 times	Served as consultant or expert/witness in major corrosion related legal cases.

Refereed Journal Publications for the Past 10 Years

(most recent listed first)

	authors	*title and source*
1.	X. Jiang, **S. Nesic**, F. Huet, B. Kinsella, B. Brown and D. Young	*"Selection of Electrode Area for Electrochemical Noise Measurements to Monitor Localized CO_2 Corrosion"*, J. Electrochemical Society, **159**, p. C283 (2012).
2.	J. Cai, C. Li, X. Tang, F. Ayello, S. Richter and **S. Nesic**	*"Experimental Study of Water Wetting in Oil–Water Two Phase Flow – Horizontal Flow of Model Oil"*, Chemical Engineering Science Journal, **73**, p. 334 (2012).
3.	M. Singer, B. Brown, A. Camacho and **S. Nesic**	*"Combined Effect of CO_2 , H_2S and Acetic Acid on Bottom of the Line Corrosion"*, J. Corrosion, **67**, No. 1, p. 1 (2011).
4.	J. Han, **S. Nesic**, Y. Yang and B. Brown	*"Spontaneous Passivation Observations During Scale Formation on Mild Steel in CO_2 Brines"*, Electrochimica Acta **56**, p. 5396 (2011).
5.	P. Ajmera, W. Robbins, S. Richter, and **S. Nesic**	*"Role of Asphaltenes in Inhibiting Corrosion and Altering the Wettability of the Steel Surface"*, J. Corrosion, **67**, No. 10, p. 1 (2011).
6.	Y.-S. Choi and **S. Nesic**	*"Determining the Corrosive Potential of CO2 Transport Pipeline in High pCO_2-water Environments"*, International Journal of Greenhouse Gas Control, **5**, p. 788 (2011).
7.	M. Singer, B. Brown, A. Camacho and **S. Nesic**	*"Sour Top-of-the-Line Corrosion in the Presence of Acetic Acid"*, J. Corrosion, **67**, No. 8, p. 1 (2011).
8.	H. Fang, B. Brown and **S. Nesic**	*"Effects of Sodium Chloride Concentration on Corrosion in Slightly Sour Environments"*, J. Corrosion, **67**, p. 1 (2011).

9. Y.-S. Choi, **S. Nesic** and S. Ling — *"Effect of H_2S on the CO_2 Corrosion of Carbon Steel in Acidic Solutions"*, Electrochimica Acta, **56**, p. 1752 (2011).

10. Y.-S. Choi, D. Duan, **S. Nesic**, F. Vitse, S. Bedell and C. Worley — *"Effect of Oxygen and Heat Stable Salts on the Corrosion of Carbon Steel in MDEA-Based CO_2 Capture Process"*, J. Corrosion, **66**, p. 4 (2010).

11. Y.-S. Choi, **S. Nesic** and D. Young — *"Effect of Impurities on the Corrosion Behavior of CO_2 Transmission Pipeline Steel in Supercritical CO_2-Water Environments"*, J. Environ. Sci. Technol., **44**, p. 9233 (2010).

12. J. Han, B. Brown and **S. Nesic** — *"Investigation of the Galvanic Mechanism for Localized Carbon Dioxide Corrosion Propagation Using the Artificial Pit Technique*", J. Corrosion, **66**, p. 31 (2010).

13. D. Hinkson, Z. Zhang, M. Singer and **S. Nesic** — *"Chemical Composition and Corrosiveness of the Condensate in Top-of-the-Line Corrosion*", J. Corrosion, **66**, p.22 (2010).

14. J. Han, B. Brown, D. Young, and **S. Nesic** — *"Mesh-capped probe design for direct pH measurements at an actively corroding metal surface"*, J. of Applied Electrochemistry, 40, p.683 (2010).

15. J. Han, D. Young, H. Colijn A. Tripathi and **S. Nesic** — *"Chemistry and Structure of the Passive Film on Mild Steel in CO2 Corrosion Environments"*, J. Industrial and Engineering Chemistry Research, **48**, p. 6296 (2009).

16. F. Farelas, M. Galicia, B. Brown, **S. Nesic** and H. Castaneda — *"Evolution of dissolution processes at the interface of carbon steel corroding in a CO_2 environment studied by EIS"*, Corrosion Science **52**, p. 509 (2009).

17. W. Sun and **S. Nesic** — *"A Mechanistic Model of Uniform Hydrogen Sulfide/Carbon Dioxide Corrosion of Mild Steel"*, J. Corrosion, **65,** p.291 (2009).

18. P. C. Okafor B. Brown and **S. Nesic** — *"CO_2 Corrosion of Carbon Steel in The Presence of Acetic Acid at Higher Temperatures"*, J. of Applied Electrochemistry, **10**, p. 873 (2009).

19. W. Sun, **S. Nesic** and R.C. Woollam — *"The Effect of Temperature and Ionic Strength on Iron Carbonate ($FeCO_3$) Solubility Limit"*, Corrosion Science **51**, p. 1273 (2009).

20. W. Sun and **S. Nesic** — *"Kinetics of Corrosion Layer Formation, Part 1. Iron Carbonate Layers in Carbon Dioxide Corrosion"*, J. Corrosion, **64,** p.334 (2008).

21. W. Sun **S. Nesic**, and S. Papavinasam — *"Kinetics of Corrosion Layer Formation, Part 2. Iron Sulfide and Mixed Iron Sulfide/Carbonate Layers in Carbon Dioxide/Hydrogen Sulfide Corrosion"*, J. Corrosion, **64,** p.586 (2008).

22. K. Chokshi, W. Sun and **S. Nesic** — *"An Investigation of Corrosion Inhibitor - Iron Carbonate Scale Interaction in Carbon Dioxide Corrosion"*, J. Corrosion Science & Engineering, **10**, preprint 24, (2008)

23. W. Sun, **S. Nesic**, D. Young and R.C. Woollam — *"Equilibrium Expressions Related to the Solubility of the Sour Corrosion Product Mackinawite"*, J. Industrial and Engineering Chemistry Research, **47**, p. 1738 (2008).

24. Z. Zhang, D. Hinkson, M. Singer, H. Wang and **S. Nesic** — *"A Mechanistic Model of Top of the Line Corrosion"*, J. Corrosion, **63,** p.1051 (2007).

25. **S. Nesic** — *"Key issues related to modelling of internal corrosion of oil and gas pipelines – A review"*, Corrosion Science, **49**, p.4308 (2007).

26. K. S. George and **S. Nesic** — *"Investigation of Carbon Dioxide Corrosion of Mild Steel in the Presence of Acetic Acid, Part I - Basic Mechanisms"*, J. Corrosion, **63,** p.178 (2007).

27. V. Ruzic, M. Veidt and **S. Nesic** — *"Protective Iron Carbonate Films – Part 3: Combined Chemo-Mechanical Removal in Single-Phase Aqueous Flow"*, J. Corrosion, **63,** p.758 (2007).

28. R. Malka, **S. Nesic** and D. A. Gulino — *"Erosion Corrosion and Synergistic Effects in Disturbed Liquid-Particle Flow"*, J. Wear, **262**, p.791 (2007).

29. S. Hernández, **S. Nesic**, G. Weckman, and V. Ghai — *"Use of Artificial Neural Networks for Predicting Crude Oil Effect on Carbon Dioxide Corrosion of Carbon Steels"*, J. Corrosion, **62**, p.467 (2006).

30. **S. Nesic** — *"Using Computational Fluid Dynamics in Combating Erosion-Corrosion"*, Chemical Engineering Science Journal, **61**, *12*, p. 4086 (2006).

31. V. Ruzic, M. Veidt and **S. Nesic** — *"Protective Iron Carbonate Films – Part 2: Chemical Removal by Dissolution in Single-Phase Aqueous Flow"*, J. Corrosion, **62,** p.598 (2006).

32. V. Ruzic, M. Veidt and **S. Nesic** — *"Protective Iron Carbonate Films – Part 1: Mechanical Removal by Hydrodynamic Forces"*, J. Corrosion, **62,** p.420 (2006).

33. P. C. Okafor and **S. Nesic** — *"Effect of Acetic Acid on CO2 Corrosion of Carbon Steel in Vapor-Water Two-Phase Horizontal Flow"*, Chem. Eng. Comm., **194**, p.141 (2006).

34. R. O. Rihan and **S. Nesic** — *"Erosion–corrosion of mild steel in hot caustic. Part I: NaOH solution"*, Corrosion Science, **48,** p.2633 (2006).

35. R. O. Rihan and **S. Nesic** — *"Erosion–corrosion of mild steel in hot caustic. Part II: the effect of acid cleaning"*, Corrosion Science, **48,** p. 2660 (2006).

36. **S. Nesic**, S. Wang, J. Cai and Y. Xiao — *"Integrated CO_2 Corrosion and Multiphase Flow Model"*, Journal of Petroleum Technology, p.48 (2004)

37. A. Keating, U. Piomelli, K. Bremhorst and **S. Nesic** — *"Large-eddy simulation of heat transfer downstream of a backward-facing step"*, Journal of Turbulence, **5** (2004).

38. F. Vitse, **S. Nesic**, Y. Gunaltun, D. L. de Torreben and P. Duchet-Suchaux — *"Mechanistic Model for the Prediction of Top-of-the-Line Corrosion Risk"*, J. Corrosion, **59,** p.1075 (2003).

39. **S. Nesic** and F. Carroll — "*A Study of The Effect of Water Wetting on CO_2 Corrosion – Using a Horizontal Rotating Cylinder*", J. Corrosion, **59,** p.1085 (2003).

40. **S. Nesic** and K.-L. Lee — "*A Mechanistic Model for CO_2 Corrosion of Mild Steel in the Presence of Protective Iron Carbonate Films – Part III: The Film Growth Model*", J. Corrosion, **59,** p. 616 (2003).

41. **S. Nesic**, M. Nordsveen, R. Nyborg and A. Stangeland — "*A Mechanistic Model for CO_2 Corrosion in the Presence of Protective Iron Carbonate Films – Part II: the Numerical Experiment*", J. Corrosion, **59** p. 489 (2003).

42. M. Nordsveen, **S. Nesic**, R. Nyborg and A. Stangeland — "*A Mechanistic Model for CO_2 Corrosion in the Presence of Protective Iron Carbonate Films – Part I: Theory and Verification*", J. Corrosion, **59,** p. 443 (2003).

43. K.-S. Yang, J.-Y. Hwang, K. Bremhorst and **S. Nesic** — *"Numerical Investigation of Turbulent Flow around a Rotating Stepped Cylinder for Corrosion Study"*, Can. J. Chemical Engineering **81**, p. 26 (2003).

Articles in Books and Monographs for the Past 10 Years

(most recent listed first)

	authors	*title and source*
1.	**S. Nesic**	*"Carbon Dioxide Corrosion of Mild Steel"*, Uhlig's Corrosion Handbook, 3rd edition, edited by W. Revie, p. 229, John Wiley and Sons Inc. (2011).
2.	J. Postlethwaite and **S. Nesic**	*"Erosion-Corrosion in Single and Multiphase Flow"*, Uhlig's Corrosion Handbook, 3rd edition, edited by W. Revie, p. 215, John Wiley and Sons Inc. (2011).
3.	J. Postlethwaite and **S. Nesic**	*"Erosion-Corrosion Recognition and Control"*, Uhlig's Corrosion Handbook, 3rd edition, edited by W. Revie, p. 907, John Wiley and Sons Inc. (2011).
4.	**S. Nesic** and W. Sun	*"Acid Gas Corrosion"*, Shrier's Corrosion, 2nd edition, edited by J. A. Richardson et. Al., Vol. 2, p. 1270, Elsevier (2010).
5.	J. Postlethwaite and **S. Nesic**	*"Erosion-Corrosion in Single and Multiphase Flow"*, Chinese edition of Uhlig's Corrosion Handbook, 2nd edition, Edited by W. Revie, Chemical Industry Press, Beijing, China (2005).

Conference Papers for the Past 10 Years

(most recent listed first)

	authors	*title and source*
1.	M. Singer, A. Camacho, B. Brown and **S. Nesic**	*"Sour Top of the Line Corrosion in the Presence of Acetic Acid"*, NACE Corrosion/2010 Conference, #10100, Houston, Texas, 2010.
2.	D. Duan, Y.-S. Choi, **S. Nesic**, F. Vitse, S. Bedell and C. Worley	*"Effect of Oxygen and Heat Stable Salts on the Corrosion of Carbon Steel in MDEA-Based CO_2 Capture Process"*, NACE Corrosion/2010 Conference, #10194, Houston, Texas, 2010.
3.	H. Fang, B. Brown and **S. Nesic**	*"High Salt Concentration Effects on CO2 Corrosion and H_2S Corrosion"*, NACE Corrosion/2010 Conference, #10276, Houston, Texas, 2010.
4.	G. M. Bota, D. Qu and **S. Nesic**	*"Naphthenic Acid Corrosion of Mild Steel in the Presence of Sulfide Scales Formed in Crude Oil Fractions at High Temperatures"*, NACE Corrosion/2010 Conference, #10353, Houston, Texas, 2010.
5.	J. Huang, B. Brown, X. Jiang, B. Kinsella and **S. Nesic**	*"Internal CO_2 Corrosion of Mild Steel Pipelines Under Inert Solid Deposits"*, NACE Corrosion/2010 Conference, #10379, Houston, Texas, 2010.
6.	P. Ajmera, W. Robbins, S. Richter and **S. Nesic**	*"The Role of Asphaltenes in Inhibiting Corrosion and Altering the Wettability of the Steel Surface"*, NACE Corrosion/2010 Conference, #10329, Houston, Texas, 2010.
7.	Y. Yang, B. Brown, **S. Nesic**, M. E. Gennaro and B. Molinas	*"Mechanical Strength and Removal of a Protective Iron Carbonate Layer Formed on Mild Steel in CO_2 Corrosion"*, NACE Corrosion/2010 Conference, #10383, Houston, Texas, 2010.
8.	T. Gu, K. Zhao and **S. Nesic**	*"A Practical Mechanistic Model for MIC Based on a Biocatalytic Cathodic Sulfate Reduction (BCSR) Theory"*, NACE Corrosion/2009 Conference, paper # 09390, Houston, USA, 2009.

9. Y-S Choi and **S. Nesic**
"*Corrosion Behavior of Carbon Steel in Supercritical CO_2 – Water Environments*", NACE Corrosion/2009 Conference, paper # 09256, Houston, USA, 2009.

10. M. Singer, D. Hinkson, Z. Zhang, H. Wang and **S. Nesic**
"*CO_2 Top of the Line Corrosion in Presence of Acetic Acid - a Parametric Study*", NACE Corrosion/2009 Conference, paper # 09292, Houston, USA, 2009.

11. H. Li, J. Huang, D. Sormaz and **S. Nesic**
"*A Free Open Source Mechanistic Model for CO_2 /H_2S Corrosion of Carbon Steel*", NACE Corrosion/2009 Conference, paper # 09572, Houston, USA, 2009.

12. X. Jiang, **S. Nesic** and F. Huet
"*The Effect of Electrode Size on Electrochemical Noise Measurements and the Role of Cl^- on Localized Corrosion for Mild Steel in CO_2 Corrosion Environment*", NACE Corrosion/2009 Conference, paper # 09575, Houston, USA, 2009.

13. Y. Yang, B. Brown and **S. Nesic**
"*Application of EQCM to the Study of CO_2 Corrosion*" Paper #4071, 17th International Corrosion Congress, Las Vegas, NV, October 6-10, 2008.

14. J. Han, B. Brown and **S. Nesic**
"*Galvanic Model for Localized CO_2 Corrosion*" Paper #2687, 17th International Corrosion Congress, Las Vegas, NV, October 6-10, 2008.

15. B. Brown, D. Young and **S. Nesic**
"*Localized Corrosion in an H_2S/CO_2 Environment*" Paper #2704, 17th International Corrosion Congress, Las Vegas, NV, October 6-10, 2008.

16. F. Ayello, W. Robbins, S. Richter and **S. Nesic**
"*Crude Oil Chemistry Effects on Inhibition of Corrosion and Phase Wetting*" Paper #3149, 17th International Corrosion Congress, Las Vegas, NV, October 6-10, 2008.

17. X. Jiang and **S. Nesic**
"*Electrochemical Investigation of the Role of Cl^- on Localized CO_2 Corrosion of Mild Steel*," Paper #2414, 17th International Corrosion Congress, Las Vegas, NV, October 6-10, 2008.

18. J. Han, D. Young and **S. Nesic**
"*Characterization of the Passive Film on Mild Steel in CO_2 Environments*" Paper #2511, 17th International Corrosion Congress, Las Vegas, NV, October 6-10, 2008.

19. H. Fang, D. Young and **S. Nesic**
"*Elemental Sulfur corrosion of Mild Steel at High Concentrations of Sodium Chloride*" Paper #2592, 17th International Corrosion Congress, Las Vegas, NV, October 6-10, 2008.

20. H. Li, J. Huang, D. Sormaz and **S. Nesic** — "*A Free Open Source Mechanistic Model for Prediction of Mild Steel Corrosion*" Paper #2659, 17th International Corrosion Congress, Las Vegas, NV, October 6-10, 2008.

21. C. Li, S. Richter and **S. Nesic** — "*Effect of Corrosion Inhibitor on Water Wetting & CO2 Corrosion in an Oil-Water Two Phase System*" Paper #2662, 17th International Corrosion Congress, Las Vegas, NV, October 6-10, 2008.

22. D. Qu, V. Kanukuntla, **S. Nesic** and A. Wolf — "*Experimental Study of Concurrent Naphthenic Acid and Sulfidation Corrosion*" Paper #2764, 17th International Corrosion Congress, Las Vegas, NV, October 6-10, 2008.

23. X. Tang, S. Richter and **S. Nesic** — "*Study of Wettability of Different Mild Steel Surfaces*" Paper #3109, 17th International Corrosion Congress, Las Vegas, NV, October 6-10, 2008.

24. **S. Nesic** — "*Mechanistic Modeling of Localized CO_2 Corrosion of Mild Steel*", Gordon Research Conference on Aqueous Corrosion, New Hampshire, USA, 2008.

25. **S. Nesic**, S. Wang, H. Fang, W. Sun and J. K-L. Lee — "*A New Updated Model of CO_2 / H_2S Corrosion in Multiphase Flow*", NACE Corrosion/2008 Conference, paper #535, Houston, USA, 2008.

26. H. Fang, D. Young and **S. Nesic** — "*Corrosion of Mild Steel in the Presence of Elemental Sulfur*", NACE Corrosion/2008 Conference, paper #637, Houston, USA, 2008.

27. J. Addis, B. Brown and **S. Nesic** — "*Erosion-Corrosion in Disturbed Liquid/Particle Flow*", NACE Corrosion/2008 Conference, paper #572, Houston, USA, 2008.

28. D. Hinkson, Z. Zhang, M. Singer and **S. Nesic** — "*A Study of the Chemical Composition and Corrosivity of the Condensate in Top of the Line Corrosion*", NACE Corrosion/2008 Conference, paper #466, Houston, USA, 2008.

29. A. Camacho, M. Singer, B. Brown, **S. Nesic** — "*Top of the Line Corrosion in H_2S / CO_2 Environments*", NACE Corrosion/2008 Conference, paper #470, Houston, USA, 2008.

30. V. Fajardo, C. Canto, B. Brown D. Young and **S. Nesic** — "*The Effect of Acetic Acid on the Integrity of Protective Iron Carbonate Layers in CO_2 Corrosion of Mild Steel*", NACE Corrosion/2008 Conference, paper #333, Houston, USA, 2008.

31. J. Han, Y. Yang, **S. Nesic** and B. Brown — "*Roles of Passivation and Galvanic Effects in Localized CO_2 Corrosion of Mild Steel*", NACE Corrosion/2008 Conference, paper #332, Houston, USA, 2008.

32. Z. Zhang, D. Hinkson, M. Singer, H. Wang and **S. Nesic** — "*A Mechanistic Model of Top of the Line Corrosion*", NACE Corrosion/2007 Conference, paper #556, Houston, USA, 2007.

33. M. Singer, B. Brown, A. Camacho and **S. Nesic** — "*Combined Effect of CO_2, H_2S and Acetic Acid on Bottom of the Line Corrosion*", NACE Corrosion/2007 Conference, paper #661, Houston, USA, 2007.

34. X. Tang, C. Li, F. Ayello, J. Cai, **S. Nesic,** C.I.T. Cruz and J. N. Al-Khamis — "*Effect Of Oil Type on Phase Wetting Transition and Corrosion in Oil-Water Flow*", NACE Corrosion/2007 Conference, paper #170, Houston, USA, 2007.

35. V. Fajardo, C. Canto, B. Brown and **S. Nesic** — "*Effect of Organic Acids in CO_2 Corrosion*", NACE Corrosion/2007 Conference, paper #319, Houston, USA, 2007.

36. J. Han, Y. Yang, B. Brown and **S. Nesic** — "*Electrochemical Investigation of Localized CO_2 Corrosion on Mild Steel*", NACE Corrosion/2007 Conference, paper #323, Houston, USA, 2007.

37. F. Ayello, X. Tang, C. Li, J. Cai, **S. Nesic,** C.I.T. Cruz and J. N. Al-Khamis — "*Determination of Phase Wetting in Oil–Water Pipe Flows*", 16th Australasian Fluids Mechanics Conference, Gold Coast, Australia, 2007.

38. **S. Nesic,** H. Fang, W. Sun and J. K-L. Lee — "*Some New Developments in Modeling of Internal Pipeline Corrosion in the Oil and Gas Industry*", Corrosion Control 007, ACA, Australia, 2007.

39. Jie Wen, Tingyue Gu and **S. Nesic** — "*Investigation of the Effects of Fluid Flow on SRB Biofilm and MIC*", NACE Corrosion/2007 Conference, paper #516, Houston, USA, 2007.

40. Burzin Khajotia, Dusan Sormaz and **S. Nesic** — "*Case-based Reasoning Model of CO_2 Corrosion Based on Field Data*", NACE Corrosion/2007 Conference, paper #553, Houston, USA, 2007.

41. W. Sun, and **S. Nesic** — "*A Mechanistic Model Of H_2S Corrosion Of Mild Steel*", NACE Corrosion/2007 Conference, paper #655, Houston, USA, 2007.

42. W. Sun, and **S. Nesic** — *"Basics Revisited: Kinetics Of Iron Carbonate Scale Precipitation In CO_2 Corrosion"*, NACE Corrosion/2006 Conference, paper #365, Houston, USA, 2006.

43. H. Fang, **S. Nesic**, B. Brown, and S. Wang — "*General CO_2 Corrosion in High Salinity Brines*", NACE Corrosion/2006 Conference, paper #372, Houston, USA, 2006.

44. K.-L. Lee and **S. Nesic** — "*Use and Abuse of EIS in Studying the Mechanisms of CO_2/H_2S Corrosion of Mild Steel*", NACE Corrosion/2006 Conference, paper #417, Houston, USA, 2006.

45. H. Wang and **S. Nesic** — "*CO_2 Corrosion Model Verification Using Field Data*", NACE Corrosion/2006 Conference, paper #567, Houston, USA, 2006.

46. R. Malka, D. Gulino and **S. Nesic** — "*Erosion Corrosion and Synergistic Effects in Disturbed Liquid-Particle Flow*", NACE Corrosion/2006 Conference, paper #594, Houston, USA, 2006.

47. C. Li, X. Tang, F. Ayello, J. Cai and **S. Nesic** — *"Experimental Study on Water Wetting and CO_2 Corrosion in Oil-Water Two-Phase Flow"*, NACE Corrosion/2006 Conference, paper #595, Houston, USA, 2006.

48. W. Sun, **S. Nesic,** and S. Papavinasam — *"Kinetics of Iron Sulfide and Mixed Iron Sulfide/Carbonate Scale Precipitation in CO_2/H_2S Corrosion,* NACE Corrosion/2006 Conference, paper #644, Houston, USA, 2006.

49. J. Wen, K. Zhao, T. Gu and **S. Nesic** — *"Effects of Mass Transfer and Flow Conditions on SRB Corrosion of Mild Steel"*, NACE Corrosion/2006 Conference, paper #666, Houston, USA, 2006.

50. X. Tang, F. Ayello, C. Li, J. Cai, **S. Nesic**, C. I. T. Cruz and J. N. Al-Khamis — *"Investigation on Water Wetting in Large Diameter Horizontal and Slightly Inclined Oil-Water Pipe Flows"*, 11th NACE Middle Eastern Corrosion Conference, Bahrain, 2006.

51. C. Canto, V. Fajardo, **S. Nesic** and B. Brown — *"Effect Of Organic Acids in CO_2 Corrosion"*, 2006 Joint International Meeting of the Electrochemical Society, Cancun, Mexico, 2006.

52. V. Ruzic, M. Veidt, and **S. Nesic** — *"Mechanisms of protective $FeCO_3$ film removal in single-phase flow-accelerated CO_2 corrosion of mild steel"*, Corrosion & Prevention-2005, The Australasian Corrosion Association Inc., Kerrimuir, Australia, 2005.

53. **S. Nesic** — *"A Mechanistic Model for CO_2 Corrosion of Mild Steel"*, **Invited lecture** at the 43rd Annual Meeting of the Serbian Chemical Society, Belgrade, Serbia, 2005.

54. J. Cai, **S. Nesic**, C. Li, X. Tang, F. Ayello C.I.T. Cruz and J.N. Al-Khamis — *"Experimental Studies of Water Wetting in Large Diameter Horizontal Oil-Water Pipe Flows"*, 2005 SPE Annual Technical Conference and Exhibition, Dallas, USA, 2005.

55. **S. Nesic** — *"Key issues related to modelling of internal corrosion of oil and gas pipelines– a review"*, **Keynote Lecture**, 16th International Corrosion Congress, Chinese Society for Corrosion and Protection, Beijing, China 2005.

56. K.-L. Lee and **S. Nesic** — *"A Mechanistic Model for CO_2 Corrosion of Mild Steel in the Presence of H_2S Accompanied by Simultaneous Iron Carbonate and Iron Sulfide Film Growth"*, 16th International Corrosion Congress, Chinese Society for Corrosion and Protection, Beijing, China 2005.

57. R. Malka, **S. Nesic** and D. A. Gulino — *"Erosion corrosion and synergistic effects in disturbed liquid-particle flow"*, 16th International Corrosion Congress, Chinese Society for Corrosion and Protection, Beijing, China 2005.

58. K. Chokshi, W. Sun and **S. Nesic** — *"Study of scale formation in CO_2 corrosion of mild steel"*, 16th International Corrosion Congress, Chinese Society for Corrosion and Protection, Beijing, China 2005.

59. K.-L. Lee and **S. Nesic** — *"The Effect of Trace Amount of H_2S on CO_2 Corrosion Investigated by Using the EIS technique"*, NACE Corrosion/2005 Conference, paper #630, Houston, USA, 2005.

60. **S. Nesic**, J. Cai and K.-L. Lee — *"A Multiphase Flow and Internal Corrosion Prediction Model for Mild Steel Pipelines"*, NACE Corrosion/2005 Conference, paper #556, Houston, USA, 2005.

61. Y. Xiao and **S. Nesic** — *"A Stochastic Prediction Model of Localized CO_2 Corrosion"*, NACE Corrosion/2005 Conference, paper #57, Houston, USA, 2005.

62. C. Méndez, M. Singer, A. Camacho, S. Hernández, **S. Nesic,** Y. Gunaltun, M. Joosten Y. Sun and P. Gabbetta — *"Effect of Acetic Acid, pH and MEG on the CO_2 Top-of-the-Line Corrosion"*, NACE Corrosion/2005 Conference, paper #278, Houston, USA, 2005.

63. K. Chokshi, W. Sun and **S. Nesic** — *"Iron Carbonate Scale Growth and the Effect of Inhibition in CO_2 Corrosion of Mild Steel"*, NACE Corrosion/2005 Conference, paper #285, Houston, USA, 2005.

64. O. A. Nafday and **S. Nesic** — *"Iron Carbonate Scale Formation and CO_2 Corrosion in the Presence of Acetic Acid"*, NACE Corrosion/2005 Conference, paper #295, Houston, USA, 2005.

65. C. M. Jhobalia, A. Hu, T. Gu and **S. Nesic** — *"Biochemical Engineering Approaches to MIC"*, NACE Corrosion/2005 Conference, paper #500, Houston, USA, 2005.

66. S. Hernández, **S. Nesic**, G. Weckman and V. Ghai — *"Use of Artificial Neural Networks for Predicting Crude Oil Effect on CO_2 Corrosion of Carbon Steels"*, NACE Corrosion/2005 Conference, paper #554, Houston, USA, 2005.

67. B. Brown and **S. Nesic** — *"CO_2 / H_2S Corrosion under Scale Forming Conditions"*, NACE Corrosion/2005 Conference, paper #625, Houston, USA, 2005.

68. **S. Nesic**, W. Sun, K. Chokshi and O. Nafday — *"Formation of Protective Iron Carbonate Films on Mild Steel – Some Important Issues"*, NACE Corrosion/2004 Conference, Research in Progress Symposium, Houston, USA, 2004.

69. **S. Nesic** and S. Coles — *"Computational Fluid Dynamics Atudy of Erosion-Corrosion in Shell-and-Tube Heat Exchanger Headers"*, NACE Corrosion/2004 Conference, Research in Progress Symposium, Houston, USA, 2004.

70. **S. Nesic** — *"Modelling of Internal Corrosion of Oil and Gas Pipelines Made from Carbon Steel"*, **Invited Lecture**, Research in Progress Symposium, NACE Corrosion/2004 Conference, Houston, USA, 2004.

71. **S. Nesic**, S. Wang, J. Cai and Y. Xiao — *"Integrated CO_2 Corrosion - Multiphase Flow Model"*, NACE Corrosion/2004 Conference, paper #626, Houston, USA, 2004.

72. K.-L. Lee and **S. Nesic** — *"EIS Investigation of CO_2/H_2S Corrosion"*, NACE Corrosion/2004 Conference, paper #728, Houston, USA, 2004.

73. S. Wang, K. George and **S. Nesic** — *"High Pressure CO_2 Corrosion Electrochemistry and the Effect of Acetic Acid"*, NACE Corrosion/2004 Conference, paper #375, Houston, USA, 2004.

74. **S. Nesic**, Y. Xiao and B. F. M. Pots — *"A Quasi 2-D Localized Corrosion Model"*, NACE Corrosion/2004 Conference, paper #628, Houston, USA, 2004.

75. M. Singer, **S. Nesic** and Y. Gunaltun — *"Top of the Line Corrosion in Presence of Acetic Acid and Carbon Dioxide"*, NACE Corrosion/2004 Conference, paper #377, Houston, USA, 2004.

76. K. George, S. Wang, **S. Nesic** and C. de Waard — *"Modelling of CO_2 Corrosion of Mild Steel at High Pressures of CO_2 and in the Presence of Acetic Acid"*, NACE Corrosion/2004 Conference, paper #623, Houston, USA, 2004.

77. K. George, **S. Nesic** and C. de Waard — *"Electrochemical Investigation and Modelling of Carbon Dioxide Corrosion of Carbon Steel in the Presence of Acetic Acid"*, NACE Corrosion/2004 Conference, paper #379, Houston, USA, 2004.

78. Y. Sun and **S. Nesic** — *"A Parametric Study and Modelling of Localized CO_2 Corrosion in Horizontal Wet Gas Flow"*, NACE Corrosion/2004 Conference, paper #380, Houston, USA, 2004.

79. J. Cai, **S. Nesic** and C. de Waard — *"Modelling Of Water Wetting in Oil-Water Pipe Flow"*, NACE Corrosion/2004 Conference, paper #663, Houston, USA, 2004.

80. Bruce Brown, Shilpha Reddy Parakala and Srdjan Nesic — *"CO_2 Corrosion in the Presence of Trace Amounts Of H_2S"*, NACE Corrosion/2004 Conference, paper #736, Houston, USA, 2004.

81. **S. Nesic**, S. Wang, J. Cai and Y. Xiao — *"A New Mechanistic CO_2 Corrosion/Multiphase Flow Model"*, 1st International Symposium on Oilfield Corrosion, Aberdeen, UK, SPE (2004).

82. **S. Nesic** — *"A Critical Review of CO_2 Corrosion Modelling in the Oil and Gas Industry"*, **Keynote Lecture**, 10th NACE Middle Eastern Corrosion Conference, Bahrain, 2004.

83. J. Cai, **S. Nesic** and C. de Waard — *"Modelling of Water Wetting and he Effect of CO_2 Corrosion in Oil-Water Pipe Flows"*, 10th NACE Middle Eastern Corrosion Conference, Bahrain, 2004.

84. **S. Nesic**, S. Wang, J. Cai and Y. Xiao — *"An Integrated CO_2 Corrosion - Multiphase Flow Model"*, 10th NACE Middle Eastern Corrosion Conference, Bahrain, 2004.

85. **S. Nesic**, S. Wang, J. Cai and Y. Xiao — *"CO_2 Corrosion in Multiphase Flow Software Package"*, NACE Regional New Orleans Offshore Corrosion Conference, Houston, USA, 2003.

86. F. Vitse, **S. Nesic**, Y. M. Gunaltun, D. L. de Torrebe, and P. Duchet-Suchaux — *"Mechanistic Model for Prediction of the Top of the Line Corrosion Risk"*, NACE Corrosion/2003 Conference, paper #633, Houston, USA, 2003.

87. S. W.ang and **S. Nesic** — *"On Coupling CO_2 Corrosion and Multiphase Flow Models"*, NACE Corrosion/2003 Conference, paper #631, Houston, USA, 2003.

88. B. Brown, K.-L. Lee and **S. Nesic** — *"Corrosion in Multiphase Flow Containing Small Amounts of H_2S"*, NACE Corrosion/2003 Conference, paper #341, Houston, USA, 2003.

89. Y. Sun, K. George and **S. Nesic** — *"The Effect of Cl and Acetic Acid on Localized CO_2 Corrosion in Wet Gas Flow"*, NACE Corrosion/2003 Conference, paper #327, Houston, USA, 2003.

APPENDIX B: MATERIALS CONSULTED

Beg Bates	End Bates	Document Title / Description
n/a	n/a	John Amos - SkyTruth - Gulf Oil Spill Rate Must be Much Higher than Stated
n/a	n/a	NYT Article Reporting 5000 bbl a day NOAA Estimate
n/a	n/a	Ian MacDonald -- SkyTruth - Gulf Oil Spill - New Spill Calculation
n/a	n/a	Crone, Chiang, Wereley -- NPR - Gulf Oil Spill May Far Exceed Government, BP Estimates NPR
n/a	n/a	Crone, Chiang, Wereley -- NPR - Transcript
n/a	n/a	Congressional Hearing - Sizing Up the BP Oil Spill - Transcript (Original)
n/a	n/a	Camilli - WHOI Prepared Congressional Statement
n/a	n/a	Camilli WHOI Presentation Plan
n/a	n/a	Werely - Congressional Presentation
n/a	n/a	FRTG Press Release
n/a	n/a	FRTG - Summary Preliminary Report
n/a	n/a	FRTG -Press Release McNutt Provide Updates on Progress of Scientific Teams
n/a	n/a	FRTG - Jun 8 - Pooling Report
n/a	n/a	FRTG - Plume Team Statement
n/a	n/a	WHOI Preliminary Report
n/a	n/a	FRTG - US Scientific Team Draws on New Data
n/a	n/a	FRTG Plume Team - PIV Report (Revised)
n/a	n/a	FRTG - Refined Estimate
n/a	n/a	Deepwater Horizon - BP Oil Budget - What happened to the oil
n/a	n/a	Deepwater Horizon MC252 Gulf Incident Oil Budget
n/a	n/a	Crone - Science Express - Magnitude of the 2010 Gulf of Mexico Oil Leak
n/a	n/a	PresComm - Flow Rate - Amount

		and Fate of Oil
n/a	n/a	PresComm - BP Comments to Oct 6 Working Paper No 3 - Amount and Fate of Oil
n/a	n/a	Oil Spill Calculator - Technical Documentation
n/a	n/a	PresComm - The Amount and Fate of the Oil (Revised)
n/a	n/a	Lehr IOSC - Computing Mass Balance for the Deepwater Horizon Spill (Presented May 26, 2011)
n/a	n/a	FRTG - Assessment of Flow Rate Estimates for the Deepwater Horizon-Macondo Oil Spill - (Combined)
n/a	n/a	(May-June) Hsieh, P - Application of Transient Analysis to Macondo
n/a	n/a	Lehr IOSC Poster- Spill Response 10 Years Later
BP-HZN-2179MDL04440732	BP-HZN-2179MDL04440732	Intertek CCE & Viscosity Tables
BP-HZN-2179MDL04440977	BP-HZN-2179MDL04440977	Intertek/Westport Multi-Stage Separator Test (MST Tables) - Native
BP-HZN-2179MDL00063016	BP-HZN-2179MDL00063016	Pencor-Sample Quality Assessment - Native
BP-HZN-2179MDL00063084	BP-HZN-2179MDL00063084	Pencor-Volatile Oil Reservoir Study - Native
BP-HZN-2179MDL01608973	BP-HZN-2179MDL01609022	Schlumberger Report
BP-HZN-2179MDL01872218	BP-HZN-2179MDL01872218	Pencor Report - Native
BP-HZN-BLY00000001	BP-HZN-BLY00000193	Deepwater Horizon Accident Investigation Report
n/a	n/a	Appendix A. Transocean Deepwater Horizon Rig Incident Investigation Into the Facts and Causation (April 23, 2010)
n/a	n/a	Appendix B. Acronyms, Abbreviations and Company Names
n/a	n/a	Appendix C Macondo Well Components of Interest
n/a	n/a	Appendix D Sperry-Sun Real-time Data Pits
n/a	n/a	Appendix E Sperry-Sun Real-time

		Data Surface Parameters
n/a	n/a	Appendix F Roles and Responsibilities for Macondo Well
n/a	n/a	Appendix G Analysis Determining the Likely Source of In Flow
n/a	n/a	Appendix H-Description of the BOP Stack and Control System
n/a	n/a	Appendix I. Deepwater Horizon Investigation Fault Trees
n/a	n/a	Appendix J. Halliburton Lab Results - #73909 2
n/a	n/a	Appendix K. Laboratory Analysis of Cementing Operations on the Deepwater Horizon (from CSI Technologies)
n/a	n/a	Appendix M. Summary Report Global Analysis Of Macondo 9 78-In X 7-In Production Casing 4992 ft Water Depth GoM (for Macondo Well Investigation) (from Stress Engineering)
n/a	n/a	Appendix N. Mississippi Canyon 252 No.1 (Macondo) Basis of Design Review
n/a	n/a	Appendix O. Industry Comparison Data on Long String Casing and Casing Liners in the Macondo Well Area
n/a	n/a	Appendix P. BP Deepwater Horizon Rheliant Displacement Procedure "Macondo" OSC-G 32306 (M-I SWACO)
n/a	n/a	Appendix Q. Summary of The Effect of Spacer Fluid Composition and Placement on Negative-pressure Test
n/a	n/a	Appendix R. Fluid Compressibility Calculation
n/a	n/a	Appendix S. First Surface Indications of Well Flow and Pit Gain
n/a	n/a	Appendix T. Comparison of Events with Relevant Transocean Well Control Policies, Practices and Procedures
n/a	n/a	Appendix U. Riser Fluid Evacuation to Rig Floor

n/a	n/a	Appendix V. BP Deepwater Horizon GOM Incident Investigation Dispersion Analysis (from BakerRisk)
n/a	n/a	Appendix W. Report-Dynamic Simulations Deepwater Horizon Incident BP (from ae add energy)
n/a	n/a	Appendix X. Deepwater Horizon Blue Pod AMF System Batteries
n/a	n/a	Appendix Y. September 2009 Ã» Deepwater Horizon Follow-up Rig Audit
n/a	n/a	Appendix Z. Hydraulic analyses of BOP Control system(from Ultra Deep)
n/a	n/a	Appendix AA. Deepwater Horizon BOP Modifications Since Commissioning
n/a	n/a	DNV BOP Report Volume II Appendices
n/a	n/a	DNV Report EP030842 for BOEMRE Volume I
BP-HZN-2179MDL04440689	BP-HZN-2179MDL04440690	Intertek Constant Composition Expansion Tables 1 & 2
BP-HZN-2179MDL04440978	BP-HZN-2179MDL04440998	Intertek/Westport Multi-Stage Separator Test (Final Report)
BP-HZN-2179MDL04826982	BP-HZN-2179MDL04826982	Riser General Data Sheet
BP-HZN-2179MDL04996569	BP-HZN-2179MDL04996571	Email from Tim Lockett to Trevor Hill re RE: Plume pics with measurements
BP-HZN-2179MDL03676655	BP-HZN-2179MDL03676667	Explanation of Erosion Rates
BP-HZN-2179MDL04802942	BP-HZN-2179MDL04802949	Erosion Potential within Kinked Riser
BP-HZN-2179MDL04824968	BP-HZN-2179MDL04825017	Woodside
BP-HZN-2179MDL04877807	BP-HZN-2179MDL04877811	Escalation of Erosion within Deepwater Horizon Kinked Riser
BP-HZN-2179MDL04908567	BP-HZN-2179MDL04908568	Estimate of Dimensions
BP-HZN-2179MDL04996572	BP-HZN-2179MDL04996572	Kink-Leak-Flowrates
BP-HZN-2179MDL03349164	BP-HZN-2179MDL03349166	3823 Work Requested - Riser Vertical Oscillations

BP-HZN-2179MDL04366973	BP-HZN-2179MDL04366974	TransOcean.Riser.2010.4.23.B-1
BP-HZN-2179MDL04926107	BP-HZN-2179MDL04926107	Riser Survey 05222010_Model-1
BP-HZN-2179MDL04926108	BP-HZN-2179MDL04926108	Riser Survey 05222010_Layout-1
BP-HZN-2179MDL04996568	BP-HZN-2179MDL04996568	Progression of Horizon Riser Surveys - 2
BP-HZN-2179MDL04996573	BP-HZN-2179MDL04996573	Riser Joint 34-35
BP-HZN-2179MDL04996574	BP-HZN-2179MDL04996574	Riser Joint 35-36
BP-HZN-2179MDL04996575	BP-HZN-2179MDL04996575	Riser Joint 36-37
BP-HZN-2179MDL04996576	BP-HZN-2179MDL04996576	Riser Joint 37-38
BP-HZN-2179MDL04996577	BP-HZN-2179MDL04996577	Riser Movement Log 5-21-10
BP-HZN-2179MDL04578104	BP-HZN-2179MDL04578104	Black Oil Tables from EoS for All Temps 11June2010
CAM_CIV_0148046	CAM_CIV_0148271	DWH BOP Stack O and M manual
BP-HZN-2179MDL02172464	BP-HZN-2179MDL02172464	DW Horizon IMT ROV Ops Notes_September 19
n/a	n/a	Rebuttal Expert Report of Forrest Earl Shanks (BP)
n/a	n/a	Expert Report of Forrest Earl Shanks FINAL(BP)
n/a	n/a	Expert Report of Greg Childs (Transocean)
HAL_0048973	HAL_0048974	Sperry Sun data [oversized]
BP-HZN-BLY00087028	BP-HZN-BLY00087028	Document Produced Natively: Chart Outlining BOP Specific Events
BP-HZN-2179MDL05497207	BP-HZN-2179MDL05497208	Email from David W Moody to Mark Mazzella re Bridging Material Results (5/28/10) & Forward Plan (5/29/10)
BP-HZN-2179MDL05497212	BP-HZN-2179MDL05497212	Bridging Materials Launched
BP-HZN-2179MDL05497215	BP-HZN-2179MDL05497218	List of Items Pumped in Order of Discharge
BP-HZN-2179MDL04996564	BP-HZN-2179MDL04996564	Laser Scan Data (Hard drive BP-036255)
BP-HZN-2179MDL04549799	BP-HZN-2179MDL04549828	BOEMRE - ADDENDUM Forensic Examination of Deepwater Horizon Blowout Preventer 050311

		(*Addendum to DNV BOP*)
CAM_CIV_0018107	CAM_CIV_0018107	BOP Blind Shear Rams
CAM_CIV_0028270	CAM_CIV_0028270	BOP Blind Shear Rams Updated Lower Blade
CAM_CIV_0020865	CAM_CIV_0020865	BOP Casing Shear Rams
CAM_CIV_0020866	CAM_CIV_0020866	BOP Variable Bore Ram
TRN-INV-02887797	TRN-INV-02887797	BOP Stack External View
TRN-INV-02956057	TRN-INV-02956058	Internal Stack Up of Dimensions of BOP
BP-HZN-2179MDL04996564-1	BP-HZN-2179MDL04996564-1	Laser Scan Data (Hard drive)
BP-HZN-2179MDL07383107	BP-HZN-2179MDL07383107	Email from Steve Carmichael to Neal McCaslin and Brian Carlson re Latest Update for Q4000 and HP1 Spreadsheets
BP-HZN-2179MDL07383109	BP-HZN-2179MDL07383109	MC252 Q4000 Data with Rates
BP-HZN-2179MDL07383108	BP-HZN-2179MDL07383108	MC252 HP1 Data with Rates
n/a	n/a	Expert Report of J. J. Azar, Ph. D
BP-HZN-2179MDL06005997	BP-HZN-2179MDL06006000	Email from Jose Gonzalez to Paul Forman, et al., re FW: Q4000 Topside Flow Rate
BP-HZN-2179MDL06006001	BP-HZN-2179MDL06006008	Q4000 Erosion Analysis of Initial Topside Facilities
BP-HZN-2179MDL04833558	BP-HZN-2179MDL04833558	Kink Plume Center Detail
BP-HZN-2179MDL04833559	BP-HZN-2179MDL04833559	Kink Plume LH Detail 2
BP-HZN-2179MDL04833560	BP-HZN-2179MDL04833560	Kink Plume LH Detail
BP-HZN-2179MDL04833561	BP-HZN-2179MDL04833561	Kink plume overview
BP-HZN-2179MDL04833563	BP-HZN-2179MDL04833563	Kink Plume RH Detail
BP-HZN-2179MDL04833562	BP-HZN-2179MDL04833562	Kink Plume RH Detail Enhanced
BP-HZN-2179MDL04833555	BP-HZN-2179MDL04833555	Email from Trevor Hill to Derek Wapman re RE: Photos and videos
BP-HZN-2179MDL04833564	BP-HZN-2179MDL04833564	Riser End 80 Detail - Enhanced
BP-HZN-2179MDL04833565	BP-HZN-2179MDL04833565	Riser End 80 Detail
BP-HZN-	BP-HZN-	Riser End 90 full - Enhanced

2179MDL04833566	2179MDL04833566	
BP-HZN-2179MDL04833567	BP-HZN-2179MDL04833567	Riser End 90 full
BP-HZN-2179MDL04833568	BP-HZN-2179MDL04833568	Riser End 90 Overview - Enhanced
BP-HZN-2179MDL04833569	BP-HZN-2179MDL04833569	Riser End 90 Overview
BP-HZN-2179MDL04833570	BP-HZN-2179MDL04833570	Riser End 90 top - Enhanced
BP-HZN-2179MDL04833571	BP-HZN-2179MDL04833571	Riser End 90 top
BP-HZN-2179MDL04833572	BP-HZN-2179MDL04833572	Riser End 160 top - Enhanced
BP-HZN-2179MDL04833573	BP-HZN-2179MDL04833573	Riser End 160 top
BP-HZN-2179MDL04833574	BP-HZN-2179MDL04833574	Riser End 270 - Enhanced
BP-HZN-2179MDL04833575	BP-HZN-2179MDL04833575	Riser End 270
BP-HZN-2179MDL05086932	BP-HZN-2179MDL05086934	Email from John Nyholt to David Brookes, et al., re Riser Kink Inspection Update: 6/23
BP-HZN-2179MDL00255269	BP-HZN-2179MDL00255269	DVD containing video of a boroscopy as described in BP-HZN-2179MDL00269156
BP-HZN-2179MDL00255270	BP-HZN-2179MDL00255270	DVD containing video of a boroscopy as described in BP-HZN-2179MDL00269156
BP-HZN-2179MDL00255271	BP-HZN-2179MDL00255271	DVD containing video of a boroscopy as described in BP-HZN-2179MDL00269156
BP-HZN-2179MDL04934351	BP-HZN-2179MDL04934351	CAD Drawing of Riser Survey May 4 2010
BP-HZN-2179MDL06094683	BP-HZN-2179MDL06094686	CAD Drawing of Riser Survey May 8 2010
BP-HZN-2179MDL05871047	BP-HZN-2179MDL05871051	CAD Drawing of Riser Survey May 13 2010
BP-HZN-2179MDL00330291	BP-HZN-2179MDL00330291	20100422-072104-CH2 MILLENNIUM37.mpg
BP-HZN-2179MDL04996564	BP-HZN-2179MDL04996564	Laser scan of riser
BP-HZN-2179MDL04996564-1	BP-HZN-2179MDL04996564-1	Laser scan of riser
BP-HZN-2179MDL07147962	BP-HZN-2179MDL07147962	Laser scan of riser

BP-HZN-2179MDL07574314	BP-HZN-2179MDL07576801	BOP related photos and Laser scan Data
BP-HZN-2179MDL05022893	BP-HZN-2179MDL05022893	BOP Pressure History (BP-HZN-2179MDL05022893) (native)
BP-HZN-2179MDL06314451	BP-HZN-2179MDL06314451	BOP PT-B Data Summary 5.15.10 (BP-HZN-2179MDL06314451) (native)
BP-HZN-2179MDL01608483	BP-HZN-2179MDL01608483	BOP Pressure Summary 25Jun2010 Modified.xls
DSE031-001794	DSE031-001883	Sandia Report - DOE-NNSA Flow Analysis Studies Associated with the Oil Release following the Deepwater Horizon Accident
BP-HZN-2179MDL06393411	BP-HZN-2179MDL06393411	Flow Status Log rev2 (BP-HZN-2179MDL06393411) (native)
BP-HZN-2179MDL06743478	BP-HZN-2179MDL06743478	MC252_PT_B_301_1 (BP-HZN-2179MDL06743478) (native)
BP-HZN-2179MDL06744885	BP-HZN-2179MDL06744885	MC252_PT_B_301_2 (BP-HZN-2179MDL06744885) (native)
BP-HZN-2179MDL06742613	BP-HZN-2179MDL06742613	Q4000_MC252_PT_B_301 (BP-HZN-2179MDL06742613) (native)
BP-HZN-2179MDL06742965	BP-HZN-2179MDL06742965	Skandi_MC252_PT_B_301_1 (BP-HZN-2179MDL06742965) (native)
BP-HZN-2179MDL06744773	BP-HZN-2179MDL06744773	Skandi_MC252_PT_B_301_2 (BP-HZN-2179MDL06744773) (native)
BP-HZN-2179MDL01942110	BP-HZN-2179MDL01942117	T_Hill_Presentation_BP-HZN-2179MDL01942110.pdf
n/a	n/a	Expert Report of Nathan Bushnell
n/a	n/a	Expert Report of Ronal Dykhuizen
n/a	n/a	Expert Report of Stewart Griffiths
n/a	n/a	Expert Report of Mehran Pooladi-Darvish
ADX003-0007575	ADX003-0007577	Email from S. Black to M. Burns re RE: Daily update
TRN-INV-02822731	TRN-INV-02822731	Assessment of Wellbore Obstruction & Discussion of Method to Clear It
SDX005-0013242	SDX005-0013243	Email from R. Merewether to M. Tatro and others, June 23, 2010, Relief wells
SNL093-017659	SNL093-017661	Email from T. Hunter to M. McNutt re Re: 3rd erosion hole
BP-KPMG Database	BP-KPMG Database	HD-PCTU2 Hard Drive with DNV BOP Testing, Phase 1 Data
BP-HZN-2179MDL07574314	BP-HZN-2179MDL07576801	Hard Drive BP-HZN-2179VOL000168-001, BP-HZN-

		2179VOL0000168-002, BP-HZN-2179VOL000168-003
BP-HZN-2179MDL07576153		BP-060799 Hard Drive
BP-HZN-2179MDL07576154		BP-060803 Hard Drive
n/a	n/a	Transcript of 30(b)(6) Deposition of David McWhorter (Cameron). Taken November 15 and 16, 2012.
n/a	n/a	Transcript of 30(b)(6) Deposition of Marcia McNutt (US). Taken October 24 and 25, 2012.
n/a	n/a	Transcript of 30(b)(6) Deposition of Tom Knox (BP). Taken October 11 and 12, 2012.
n/a	n/a	Transcript of 30(b)(6) Deposition of George Guthrie (US). Taken November 15 and 16, 2012.
n/a	n/a	Transcript of Deposition of Secretary Steven Chu. Taken January 24, 2013.
n/a	n/a	Transcript of Deposition of Mark Havstad. Taken April 29, 2013.
n/a	n/a	TREX 007535: Expert Report of Gregg Perkin (PSC)
n/a	n/a	TREX 007536: Appendices to Expert Report of Gregg Perkin (PSC)
HCG586-001218	HCG586-001218	Email from T. Allen to M. Landry, June 9, 2010, RE: BREAK DOWN AND EROSION INSIDE CASING
IGS635-004603	IGS635-004605	Dep. Exh. 8852, Email from M. McNutt to M. Garcia, June 8, 2010, RE: Preliminary flow rate results
SDX010-0006269	SDX010-0006270	Dep. Exh. 9389, Flow Uncertainty Position
ETL080-009219	ETL080-009223	Dep. Exh. 9671, Email from M. McNutt to T. Hunter, Jan. 6, 2011, Re: tom hunter feedback on new data
SDX011-0012700	SDX011-0012702	Dep. Exh. 11297, Email from M. Tatro to A. Ratzel, July 26, 2010, FW: addition to calc
ERP001-004329	ERP001-004330	Dep. Exh. 11312, Email from M. McNutt to S. Chu, July 19, 2010, RE: Accurate account of flow into the Gulf.

n/a	n/a	Sand Production analysis by Hans Vaziri (attached as Appendix E)
n/a	n/a	BSR analysis by Nigel Richardson (attached as Appendix F)

APPENDIX C: CALIBRATION SIMULATION

The capability and accuracy of Fluent to predict turbulent and single-phase flow fields is well established, at least when it comes to the type of flow geometries simulated here. (The same is true for prediction of dispersed particle movement in a turbulent flow field, particularly for dilute slurries.) Because the biggest uncertainty is related to the performance of the erosion model, early on I tested and calibrated the erosion model in Fluent using a well understood flow geometry, where reliable experimental flow and erosion data exist. I selected for this purpose a well-documented flow/erosion case including pipe flow carrying 2% dispersed sand in water through a sudden constriction, groove, and sudden expansion (see Figure 35a).

Results of simulations are shown in Figure 35 - Figure 38. As fluid with entrained sand particles enters the pipe constriction, it accelerates and causes significant erosion at the leading edge (see Figure 36 and Figure 37). The complete pattern of erosion is shown in Figure 38—both the simulation results and the experimental values. After adjusting the erosion model, one can claim reasonable agreement, particularly considering that the simulation represents an instantaneous situation ("snapshot" at a given point), whereas the measurements are an averaged result obtained over 72 hours of exposure. Because of the high erosion rate of the leading edge of the sudden pipe constriction, it rapidly changes shape over the course of the long exposure, as simulated using a transient simulation with a moving mesh, seen in Figure 39. With this technique, the two-way interaction between flow and erosion is captured, and the change of shape of the eroded surface is predicted, as demonstrated in Figure 40 (showing the leading edge of the sudden pipe constriction which is eroded by 72 hours of exposure, where agreement

between the simulations and the experimental results is remarkable).[14] After this exercise, the Fluent package was ready for application to the flow geometries to be addressed in this work.

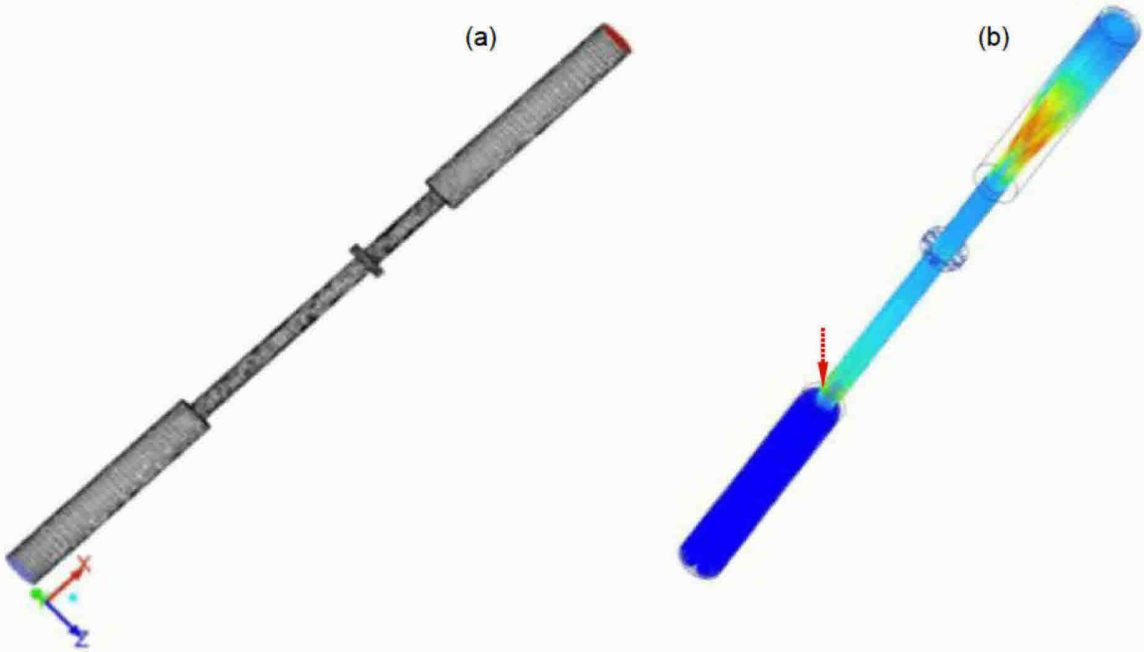

Figure 35. (a) Computational mesh and (b) fluid pathlines colored by turbulence level, for a CFD simulation of flow of water with dispersed particles through a pipe with a sudden constriction, groove, and sudden expansion, used for erosion model calibration. Red arrow points to the location of maximum erosion.

[14] Moving-mesh simulations are computer-intensive and could be executed only for simple geometries such as the one used for erosion model calibration.

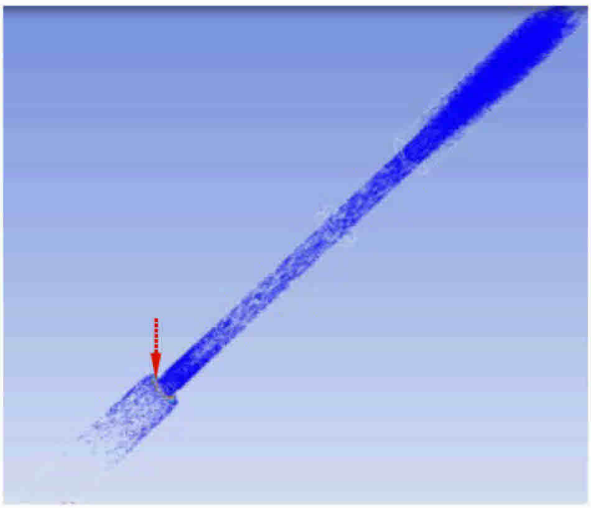

Figure 36. Particle trajectories colored by erosion level for a simulation of flow of water with dispersed particles through a pipe with a sudden constriction, groove, and sudden expansion used for erosion model calibration. Red arrow points to the same location of maximum erosion.

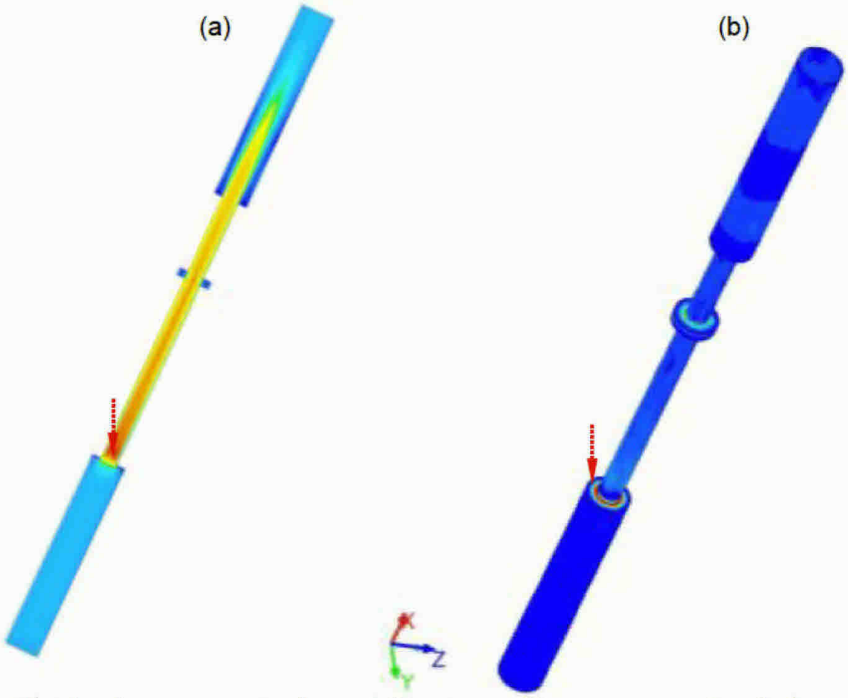

Figure 37. (a) Fluid velocity magnitude and (b) pipe wall erosion rate level, for a simulation of flow of water with dispersed particles through a pipe with a sudden constriction, groove, and sudden expansion used for erosion model calibration. Red arrow points to the same location of maximum erosion.

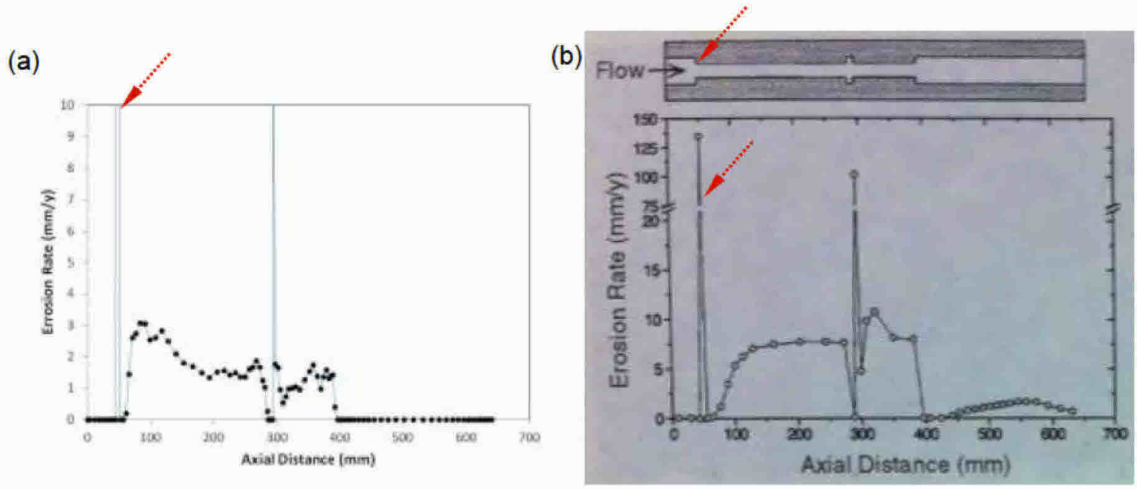

Figure 38. (a) CFD simulation results and (b) measurements of the erosion rate for a case of flow of water with dispersed particles through a pipe with a sudden constriction, groove, and sudden expansion used for erosion model calibration. Red arrow points to the same location of maximum erosion.

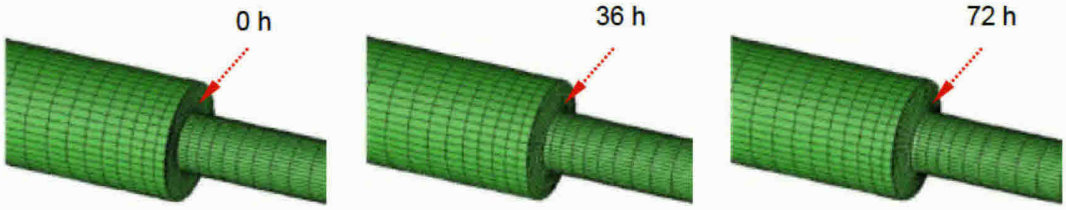

Figure 39. Transient CFD simulation results using a moving mesh, showing change of leading edge of a sudden pipe constriction due to erosion, for a case of flow of water with dispersed particles through a pipe with a sudden constriction, groove, and sudden expansion used for erosion model calibration. Red arrow points to the same location of maximum erosion.

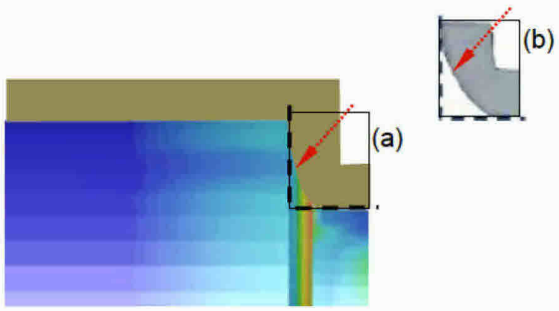

Figure 40. Detail showing eroded leading edge of sudden pipe constriction after 72 h of exposure: frame (a) is CFD simulation result and frame (b) is the experimental result, for the case of flow of water with dispersed particles through a pipe with a sudden constriction, groove, and sudden expansion used for erosion model calibration. Red arrow points to the same location of maximum erosion.

APPENDIX D: PROCESSING, IMPORTING AND MESHING CAD FILES IN FLUENT

PRE-EROSION BSR

To assemble a pre-erosion BSR flow geometry, I started with a CAD design model of the BSR blocks. Using the Siemens' NX™ CAD package, I inserted the BSR blocks into the BSR housing cavity, as shown in Figure 41 and Figure 42. Then I superimposed the wellbore pipe and the partially-severed drillpipe within the CAD model, as shown in Figure 43, to complete the pre-erosion BSR assembly.

Because my focus is on internal flow, I needed to produce a geometry of the interior cavity of the pre-erosion BSR assembly space through which fluid passed. To that end, I used the CAD package to create an "inverse" model of the initial BSR solid assembly geometry, as shown in Figure 44 and Figure 45. I then imported this inverse (flow) geometry into Fluent (Figure 46) and examined and meshed it (Figure 47) to prepare for fluid flow and erosion calculations. In the semitransparent images shown in Figure 46, one can identify the external boundaries of the flow geometry as defined by the wellbore, the internal drillpipe, and the blockage created by partially closed BSR blocks. The drill pipe, which is deformed and severed by the BSR blocks, is off-center.

(a)

(b)

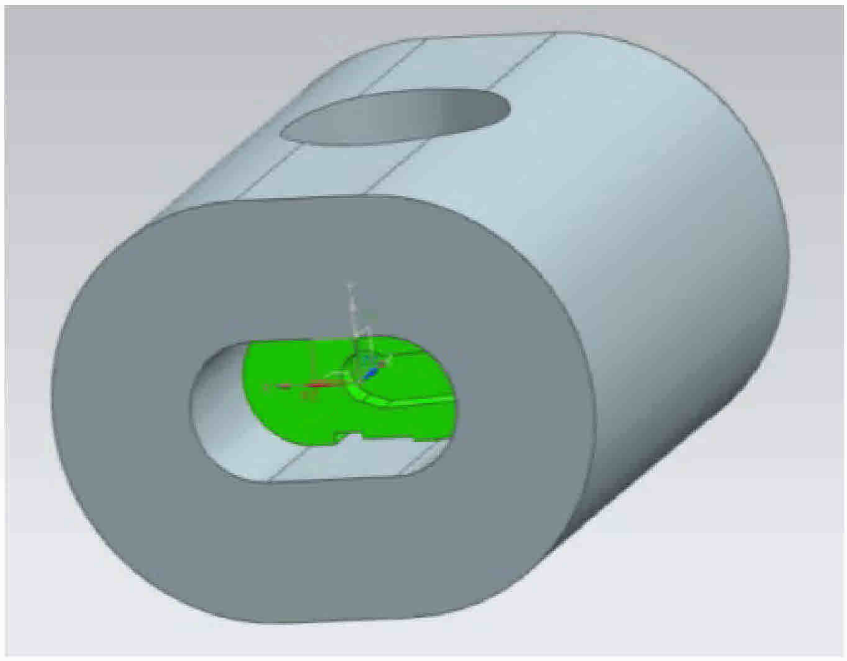

Figure 41. Opaque CAD models of (a) BSR blocks and (b) BSR blocks positioned within BSR housing cavity.

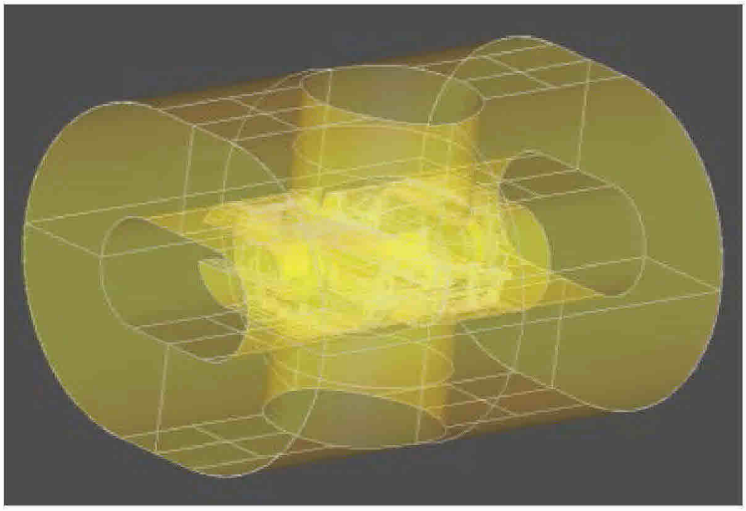

Figure 42. Semi-transparent CAD model of pre-erosion *BSR housing cavity with BSR blocks inside.*

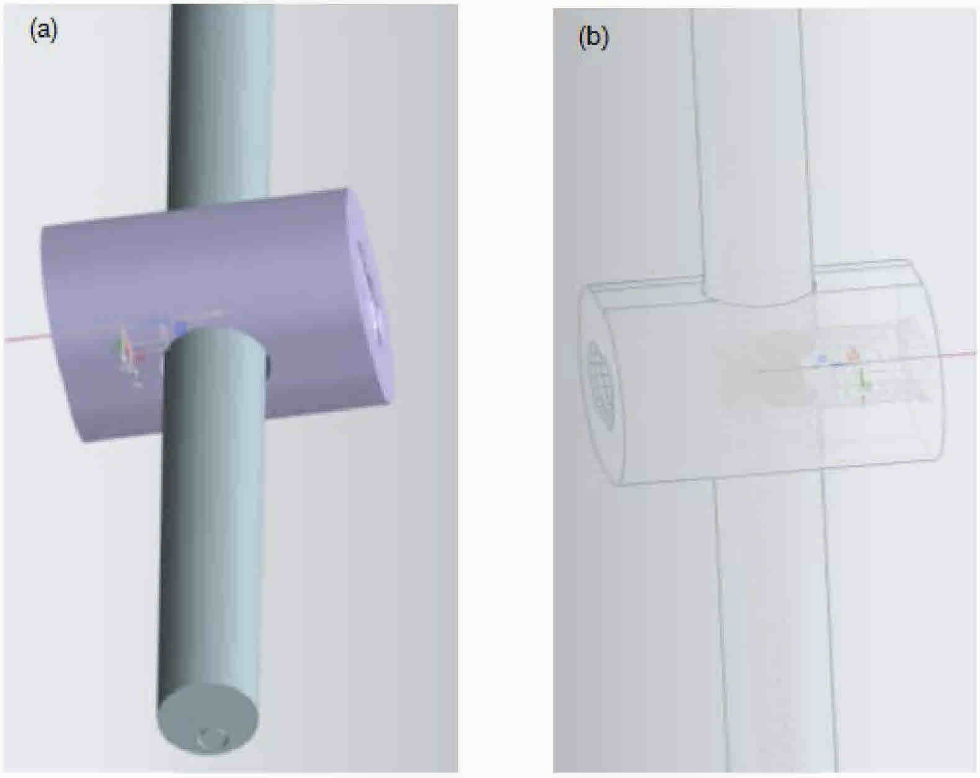

Figure 43. (a) Opaque and (b) semi-transparent CAD models of whole pre-erosion *BSR assembly, including BSR housing cavity with BSR blocks inside wellbore and off-center drillpipe.*

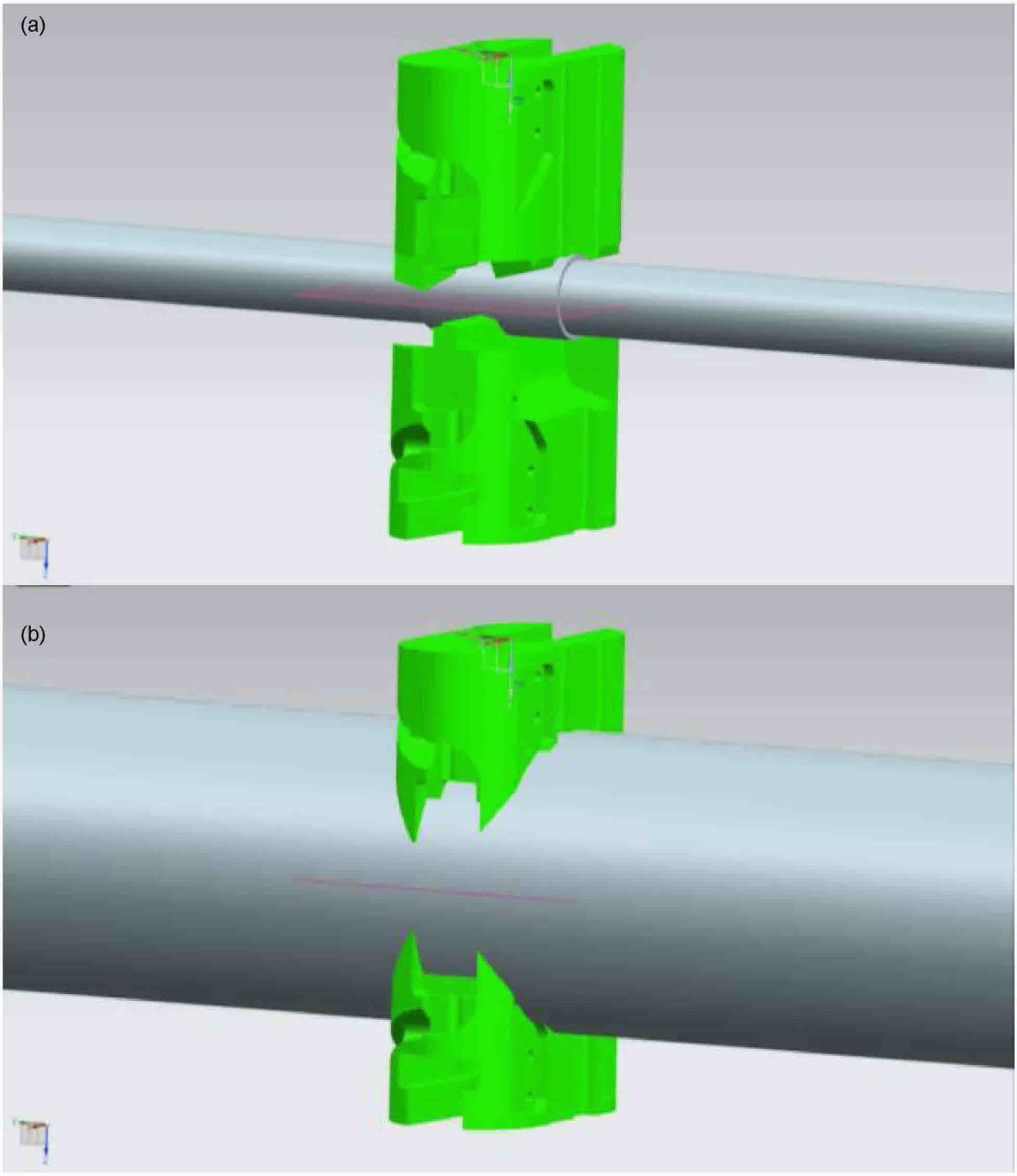

Figure 44. CAD model of BSR blocks (a) superimposed on drillpipe and (b) with wellbore superimposed.

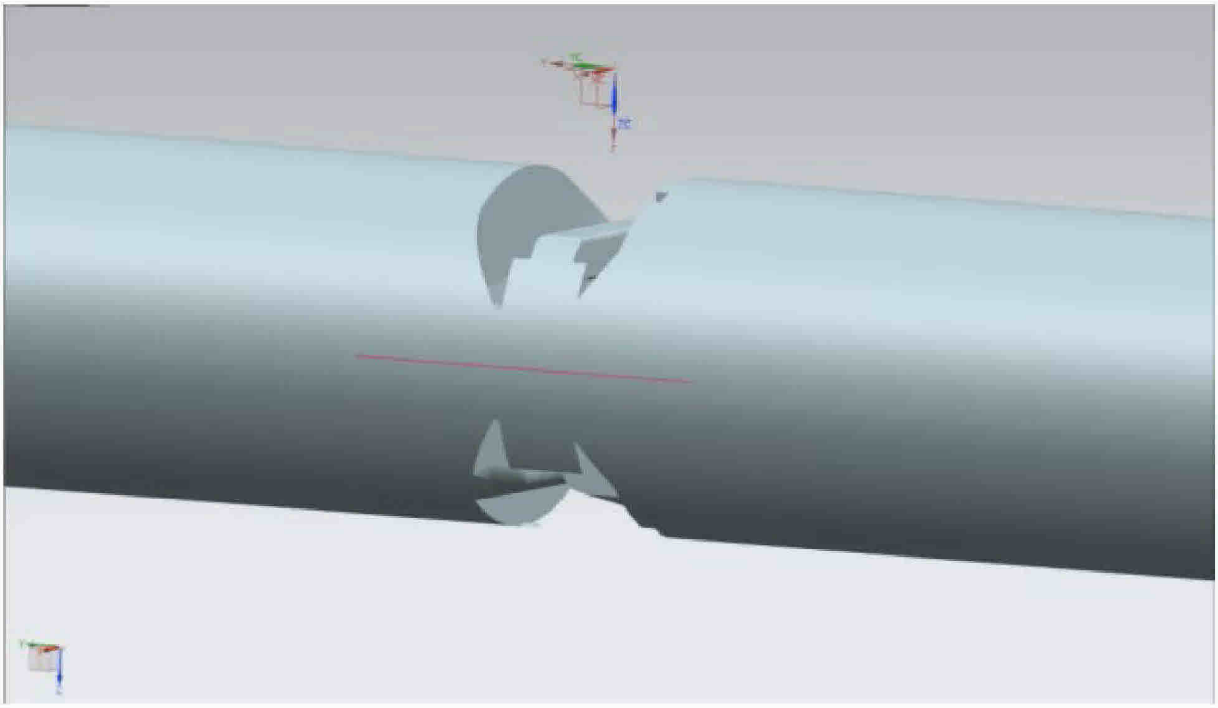

Figure 45. CAD model of "inverse" of pre-erosion *BSR assembly shown in Figure 44.*


(a)

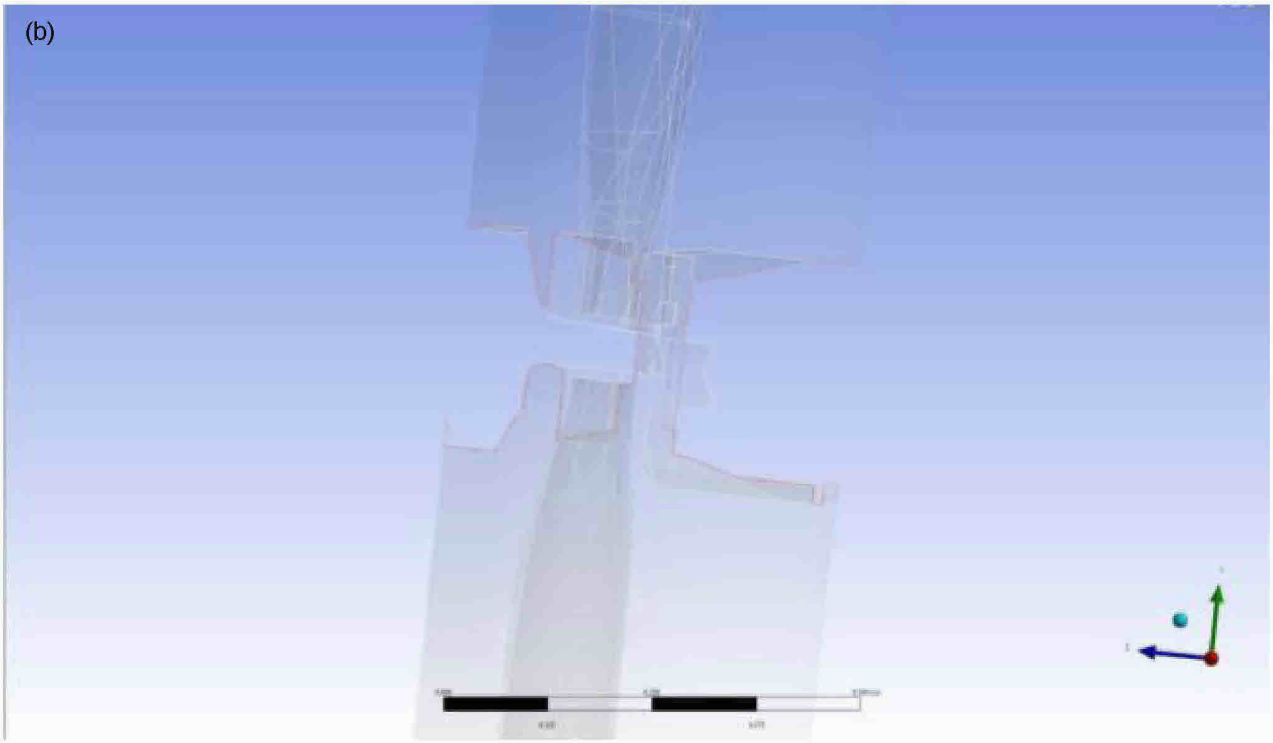
(b)

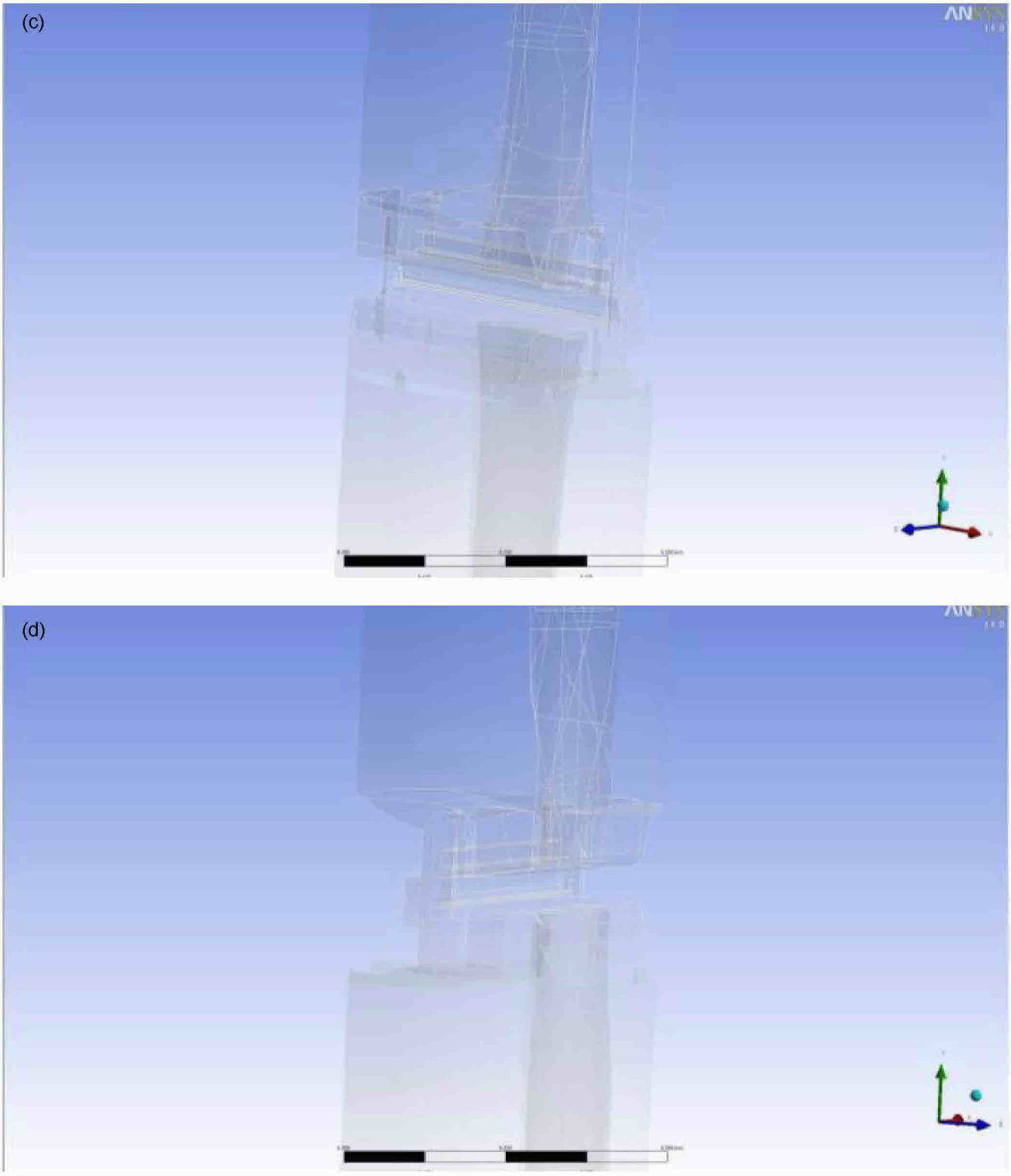

Figure 46. Different views of complete model of pre-erosion *BSR flow geometry in Fluent.*

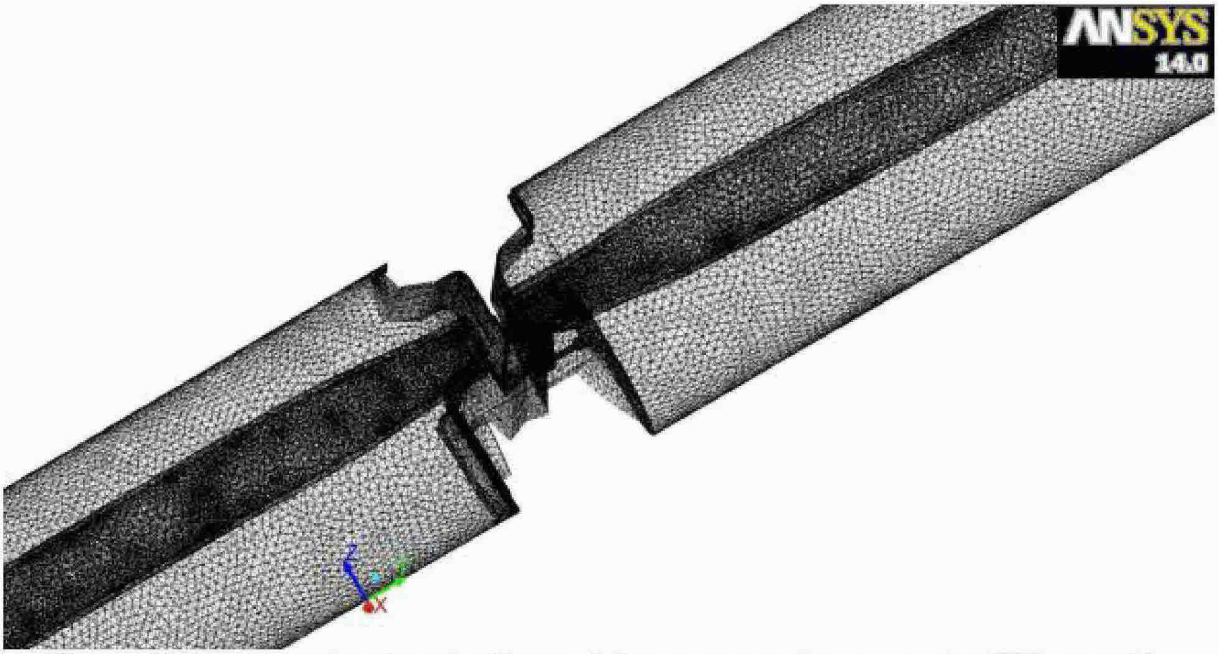

Figure 47. A computational mesh of internal flow geometry for pre-erosion BSR assembly.

POST-EROSION BSR

I next considered the geometry of the eroded BSR blocks. Specifically, I converted laser scans of the eroded BSR into CAD files and combined them with the eroded housing (see Figure 48) and repeated the whole procedure described above, this time for the post-erosion BSR blocks. The inverse CAD (flow) geometry of the post-erosion BSR blocks, which was imported into Fluent, is shown in Figure 49.

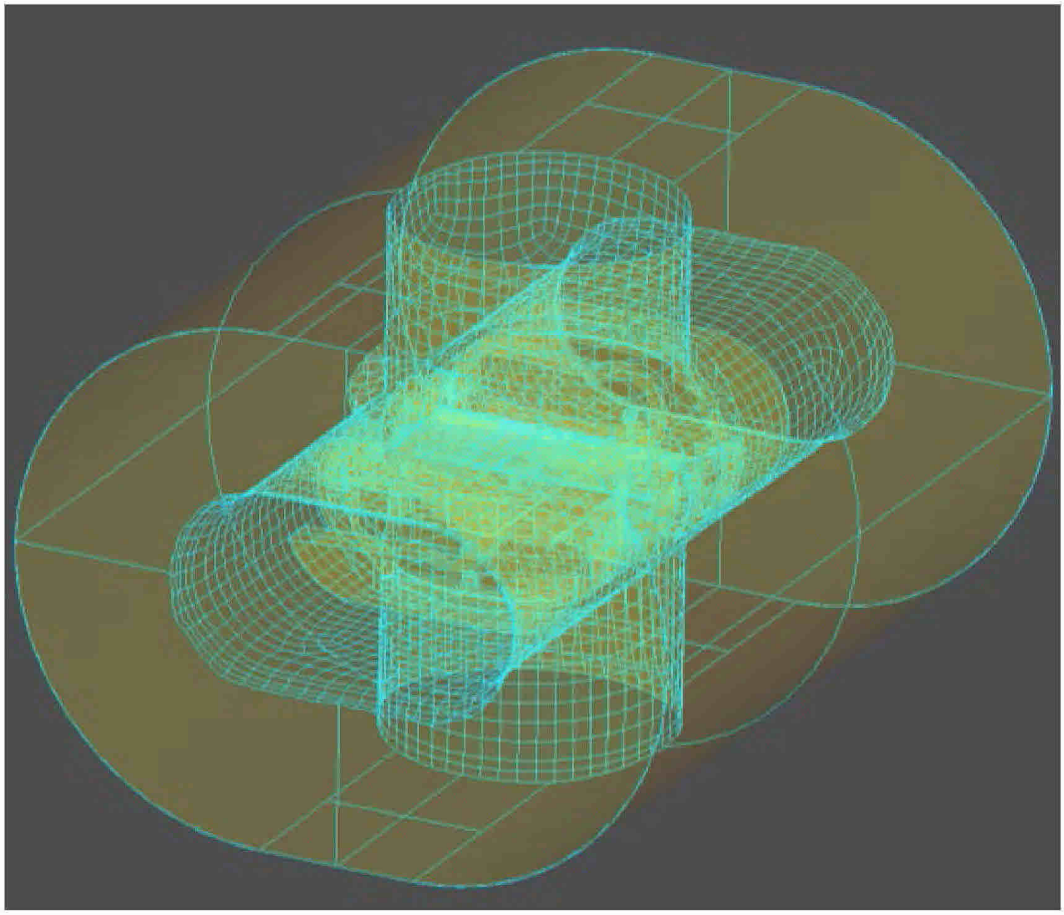

Figure 48. Semi-transparent CAD model of post-erosion *BSR housing cavity with BSR blocks inside.*

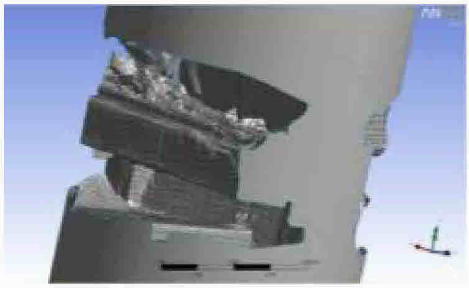

Figure 49. CAD model of "inverse" of post-erosion *BSR assembly.*

PRE-EROSION CSR

I used the same procedure to set up the pre-erosion CSR flow geometry. I started with a CAD design model of the CSR blocks (Figure 50) and superimposed the blocks with the drillpipe and the wellbore (see Figure 51). I then created the inverse (flow) geometry (Figure 52), imported the geometry into Fluent (Figure 53) and meshed (Figure 54).

Figure 50. CAD model of pre-erosion *CSR blocks.*

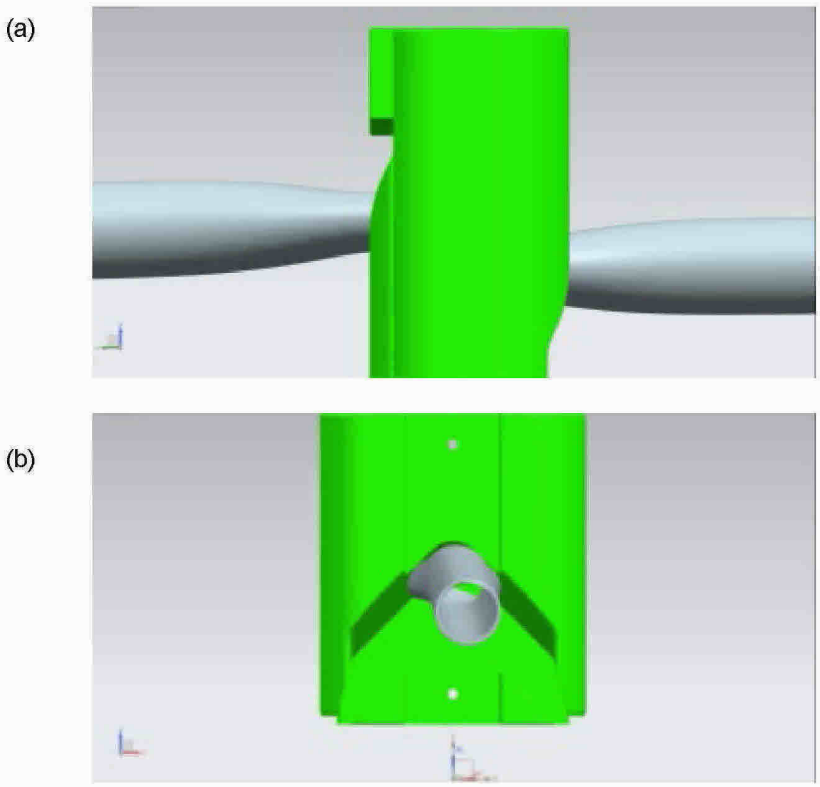

Figure 51. CAD model of pre-erosion *CSR blocks superimposed on severed drillpipe, (a) side view, and (b) top view.*

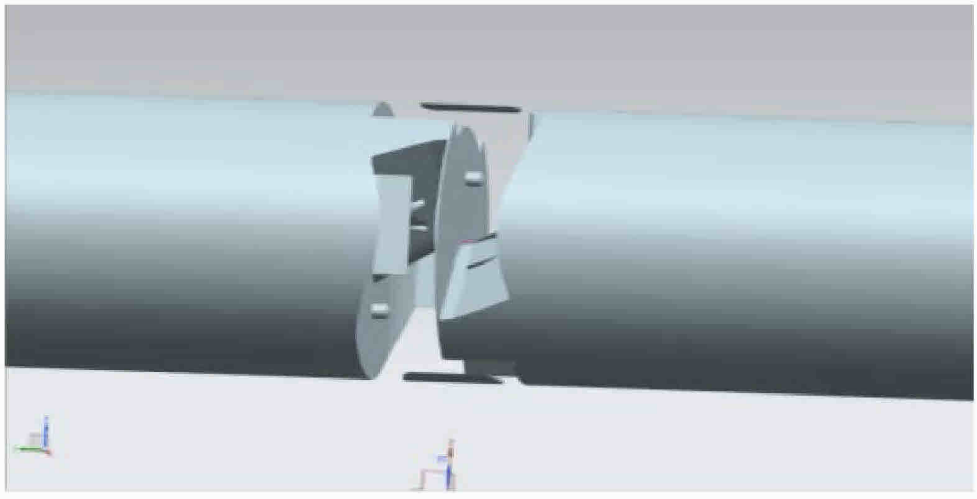

Figure 52. CAD model of "inverse" of pre-erosion *CSR assembly.*

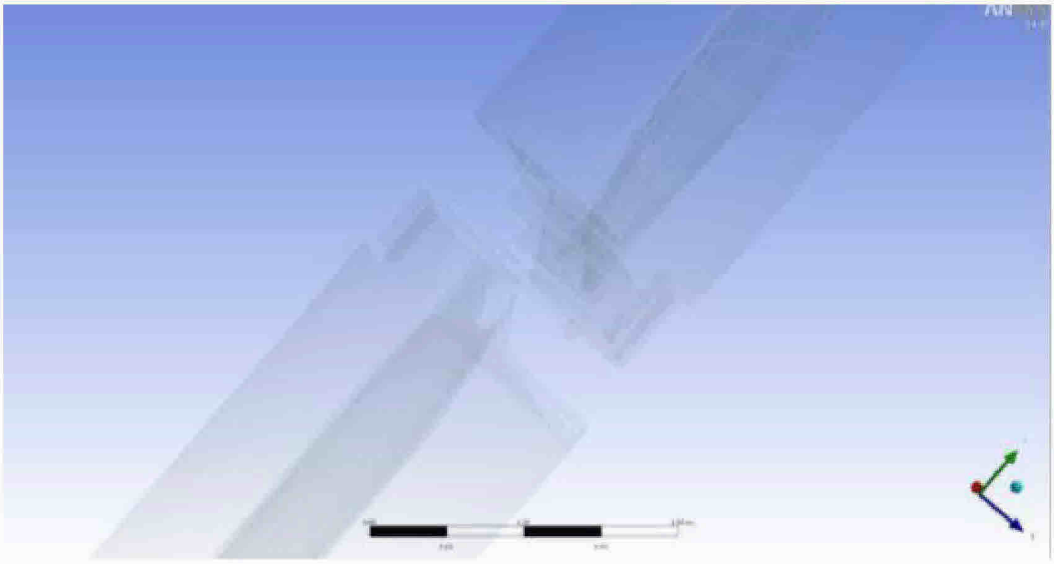

Figure 53. A complete model of pre-erosion *CSR flow geometry in Fluent.*

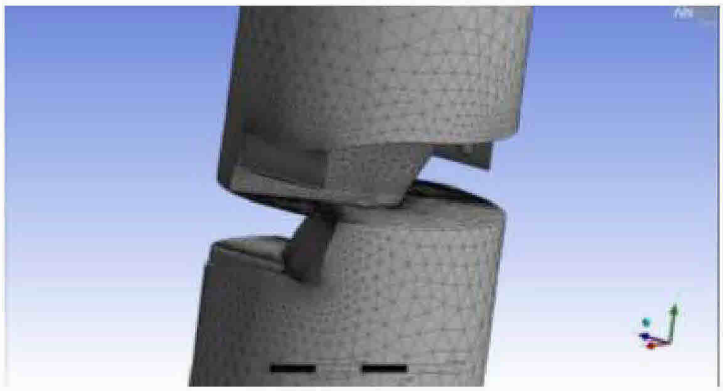

Figure 54. A computational mesh of internal flow geometry for pre-erosion *CSR assembly in Fluent.*

POST-EROSION CSR

I repeated the process for the post-erosion CSR flow geometry. I converted laser scans of the eroded CSR blocks into CAD files and imported them into the Siemens NX™ environment, where the inverse (flow) geometry was created (see Figure 55). I imported this geometry into Fluent and meshed.

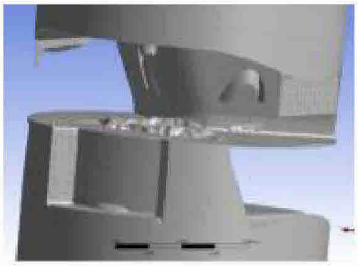

Figure 55. CAD model of the "inverse" of the post-erosion *CSR assembly.*

UA AND KINKED RISER

Construction of the simplified UAP geometry and the kinked riser geometry is described in the main body of the report.

APPENDIX E: ESTIMATION OF SAND PRODUCTION IN THE MACONDO WELL

Prepared by Hans Vaziri, Ph.D, April 30, 2013

Redacted Analysis of Relied-On Non-Testifying Expert Dr. Hans Vaziri

APPENDIX F: DRILL PIPE BUCKLING AND BLIND SHEAR RAM OPERATIONAL ANALYSIS

Prepared by Nigel Richardson, April 29, 2013

Redacted Analysis of Relied-On Non-Testifying Expert Dr. Nigel Richardson